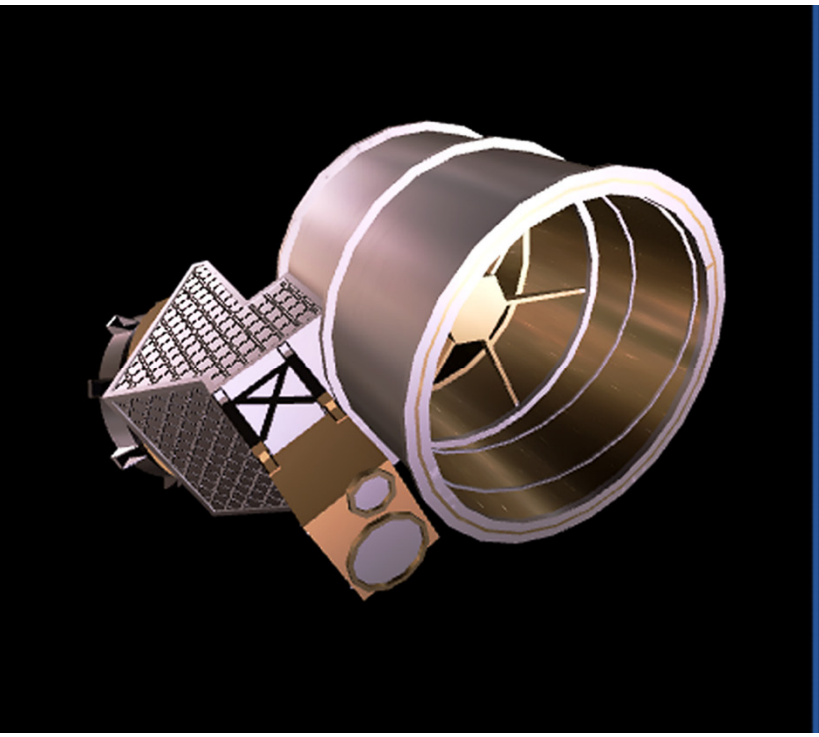

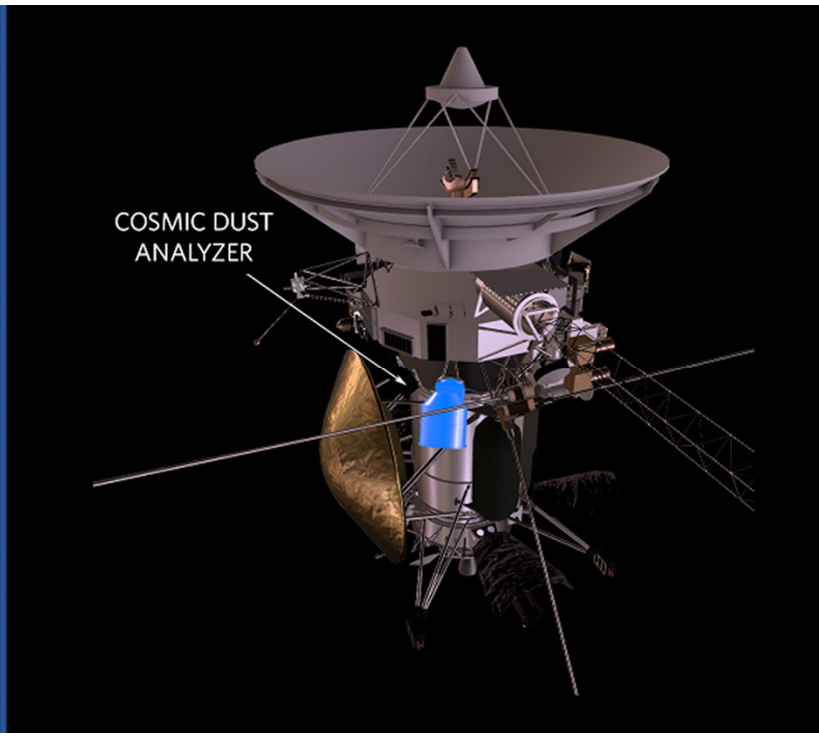

Cosmic Dust Analyzer

The Cosmic Dust Analyzer (CDA) directly sampled the composition, mass, impact direction, and speed of dust and ice particles in the Saturn system, as well as the Jupiter system and in interplanetary space. The **science objectives** of CDA included mapping the size distribution and chemical composition of ring material in the Saturn system, studying dynamical processes responsible for the diffuse E-ring structure, obtaining information on the chemical composition of satellites, and determining the role that dust plays as source and sink of charged particles in the magnetosphere.

CDA was composed of two sensors, the high-rate detectors (HRDs) designed to measure high impact rates in dust-rich environments such as ring plane crossings and the dust analyzer (DA) that measured the electric charge carried by dust particles, their impact directions, speeds, masses, and chemical composition. CDA was on an articulated mechanism that enabled the entire instrument to rotate and reposition to enable measurements of particle fluxes over a wide range of directions.

CONTENTS

Figures

Tables

EXECUTIVE SUMMARY

The science objectives of the Cassini-Huygens CDA were to carry out in situ characterization of the dust environments in order to infer properties of the dust-emitting sources as well as to study the underlying processes associated with dust. The capability to measure both the compositional and dynamical properties of incident dust grains makes the CDA measurements uniquely useful to explore the dust environment in the Saturnian system, as well as other dust populations from the Jovian system (i.e., the nanodust stream particles), and from interplanetary and interstellar space.

The CDA instrument performance over the entire time from 1999 until the last second of Cassini in September 2017 was outstanding.

At Saturn, CDA has successfully characterized the structure and the composition of Saturn's diffuse E-ring, its relation to the geologically active icy moon Enceladus, and how the E-ring interacts with the magnetosphere. CDA results contributed significantly to our understanding of Enceladus and its subsurface ocean, promoting the exploration of the habitability of the ocean worlds in the outer solar system. CDA also provided observational constraints for other diffuse rings (e.g., G-ring and Pallene ring) and the ejecta cloud around the major icy moons of Saturn. During the Grand Finale orbits, CDA detected material directly from Saturn's main rings and revealed ring-planet interactions through charged nanodust.

In addition, the dust populations arriving at the Saturnian system, i.e., interplanetary dust particles (IDPs) and interstellar dust (ISD), were also characterized thanks to the extended mission. Tiny grains expelled from both the Jovian and Saturnian systems by electromagnetic forces were also detected, providing additional information about their source moons and helping to understand the coupling between the interplanetary magnetic field (IMF) and the dynamics of these charged grains.

The CDA instrument performance over the entire time was outstanding. CDA switched on in 1999 and measured almost continuously until the last second of Cassini in September 2017. All five measurement channels (primary charge grid, targets, ion grid, and multiplier) worked the entire time. The multiplier of the spectrometer showed only a minor gain change. No issues with instrument high voltage were identified and the CDA thermal parameters were in the nominal range. The only instrument degradation that occurred was related to close Enceladus plume crossings where the gain of the two target channels decreased. This had no effect on charge or compositional measurements, instead the lower sensitivity was used to perform measurements in the dense E-ring with a higher mass threshold to avoid instrument saturation. A major concern was the Cassini pointing profile and although CDA used its articulation platform approximately once a day in order to track the dust RAM direction, many observations were not possible. Updates of the CDA flight software optimized the instrument performance during special events (Enceladus flybys). Very high impact rates required special instrument settings due to the long instrument dead time of one second. The noise behavior of CDA remained constant during the entire time and no significant interference with the spacecraft or other subsystems was observed. Only the Radio and Plasma

Wave Science (RPWS) active sounder operation led to interferences in the primary charge channel (QP) of CDA.

The major CDA findings are listed below for each science working group as well as during the cruise phase:

Rings

- The exogenous mass influx and the age of the main rings are determined.
- In situ measurement of E-ring particles shows the large extension of the ring all the way to Titan's orbit (~20 R_S).
- Charged grains are the result of dust-plasma interactions in Saturn's magnetosphere. The grain charge polarity switches from negative to positive at a radial distance of around 7 R_S as predicted by models.
- The E-ring is asymmetrical with respect to local time—it is denser and the peak locations are closer to Saturn near local noon and vice versa.

Icy satellites

- In situ characterization of the dusty plume of Enceladus.
- Discovery of the subsurface liquid water reservoir below the icy crust of Enceladus, inferred from the salt-rich E-ring ice grains.
- Ongoing hydrothermal activities within Enceladus' subsurface ocean, inferred from nano-phase silica particles.
- Discovery of complex organic molecules in ice grains from Enceladus.

Magnetosphere and plasma sciences

- Discovery of fast nanodust from Saturn.
- Fast nanograins are probes of the interplanetary magnetic field, as a result of their dynamical interactions with the interplanetary magnetic field.

Others

- Interstellar dust grains penetrate deep into the heliosphere and reach the Earth orbit. Its composition is found to be homogeneous and rich in silicates.
- Sodium chloride is the dominant constituent of the Jovian stream particles, implying they are early condensates from the volcanic plumes of Io.

- Interplanetary dust particles carry surface charges in agreement with the charging models in interplanetary space.
- In situ analysis of two metal-rich interplanetary dust particles by time-of-flight mass spectrometry (TOF MS) in the inner solar system.

CDA is the first dedicated dust instrument operated at Saturn. While its results have changed our view on the role of microscopic dust grains in the system and space exploration, several open questions remain to be resolved in the future:

- What expected ejecta clouds stemming from interplanetary micrometeorite impacts have not been detected around major icy moons (except Rhea) embedded in the E-ring?
- What is the production yield and the size distribution of impact-ejecta particles produced from Saturn's icy moons and the main rings?
- What is the original origin of silicates apparently coming from Saturn's main rings, as detected during the Grand Finale orbits?
- What, if any, are the effects on Saturn's upper atmosphere of nanograins from the main rings?
- What is the dusty plasma status in the plume of Enceladus and the core of the E-ring? What would be its impact on E-ring grain dynamics?

CDA was a highly reliable and versatile instrument with a mass sensitivity 10^6 times higher than those of the Pioneer 10 and 11 dust detectors that measured dust at Saturn prior to Cassini.

CDA Instrument Summary

The CDA was designed to provide direct observations of the impacting dust grains. CDA investigated the physical, chemical, and dynamical properties of impacting dust particles, and their interactions with satellites, rings, and Saturn's magnetosphere [Srama et al. 2004]. The chemical composition of interplanetary meteoroids was successfully compared with asteroidal and cometary dust, as well as with dust in orbit about Saturn and the ejected dust particles from rings and satellites at Saturn and during the flyby at Jupiter. The electrical charging of dust particles in the magnetosphere and the subsequent effects of the ambient plasma and magnetic fields on the trajectories of dust particles have been successfully observed by CDA.

CDA was a highly reliable and versatile instrument with a mass sensitivity 10^6 times higher than those of the Pioneer 10 and 11 dust detectors that measured dust at Saturn prior to Cassini. CDA had significant heritage from former space instrumentation developed for the Vega, Giotto, Galileo, and Ulysses missions.

CDA consisted of two independent subsystems, the High Rate Detector (HRD) and the Dust Analyzer (DA). HRD was designed to monitor high impact rates (up to 10^6 m^{-2} s^{-1}) in dust-rich environments such as during the Saturn ring plane crossings. HRD uses polyvinylidene difluoride (PVDF) foils to detect the impact energy of particles larger than approximately 1 micrometer.

The DA was sensitive to particles within a large mass range of 5×10^{-18} to 10^{-12} kg for impact speeds of ~20 km s^{-1} and covered an impact velocity range of 1 to 100 km s^{-1}, measuring the electrical charge, mass, impact velocity, and elemental composition of the impacting dust grains. This was accomplished by a suite of three DA detectors: 1) a charge sensing unit (QP) in front of the instrument; 2) a classical impact ionization detector (IID); and 3) a time-of-flight mass spectrometer (TOF MS), the chemical analyzer (CA) as a compositional mass analyzer with a mass resolution of up to 50. Both subsystems, HRD and DA, point in the same direction. The units are mounted at 45 degrees on an articulation platform with one rotation axis and an angular range of 270 degrees. The field of views of the subsystems are 180 degrees (HRD), 90 degrees (IID), and 56 degrees (CA), respectively. The instrument had a total mass of 17 kg, a data rate between 0.1 and 4 kbps, and consumed 12 W of electrical power.

Key Objectives for the CDA Instrument

The scientific goals of the Cassini dust instrument were defined as:

- **Cruise science**. Extended studies of interplanetary dust from the Earth to the orbit of Saturn. Sample the chemical composition and the charging state of dust in interplanetary space. Determine the flux of interstellar particles during solar maximum conditions. Search for dust streams originating from Saturn.
- **Jupiter flyby**. Investigate the dynamics of the Io dust streams discovered by Ulysses and Galileo. Characterize their direction, size-mass-distribution, and correlation with the Jovian and interplanetary magnetic field. Investigate the dust stream fluxes caused by the Jovian system with respect to Jupiter distance. Analyze dust stream particles at a different epoch from Galileo. Characterize the elemental composition of dust stream particles.
- **Rings**. Map size distribution of ring material, search for ring particles beyond the known E-ring. Determine the sources and sinks of E-ring dust grains. Analyze the chemical composition of ring particles. Study dynamical processes (erosional, plasma, and electromagnetic) responsible for the E-ring structure, study interactions between the E-ring and Saturn's magnetosphere, and search for electromagnetic resonances. Study ring interaction with Titan. Determine dust and meteoroid distribution both in the vicinity of the rings and in interplanetary space.
- **Icy satellites**. Define the role of meteoroid impacts as a mechanism for surface modification. Obtain information on the chemical composition of satellites from the analysis of gravitationally bound ejecta particles in the vicinity of the satellites (within Hill spheres). Investigate interactions with the ring system and determine the

importance of the various satellites as sources of ring particles. Search for particles from retrograde moons.

- **Magnetosphere of Saturn**. Determine the role that dust plays as source and sink for charged particles in the magnetosphere. Search for electromagnetically dominated dust (small particles) and for dust streams. Constrain the origin of dust streams.

CDA Science Assessment

Table CDA-1 contains an assessment of CDA science based on the objectives in the original Announcement of Opportunity (AO) and the Cassini Traceability Matrix (TM) developed for the Equinox and Solstice missions. The key AO and TM objectives addressed are:

- **Cruise Interplanetary Dust Studies (C_AO4)** – Extend studies of interplanetary dust to the orbit of Saturn.
- **Icy Satellite Geology and History (I_AO1)** – Determine the general characteristics and geological histories of the satellites.
- **Icy Satellite Surface and Crustal Modifications (I_AO2)** – Define the mechanisms of crustal and surface modifications, both external and internal.
- **Icy Satellite Surface Composition (I_AO3)** – Investigate the compositions and distributions of surface materials, particularly dark, organic-rich materials and low melting point condensed volatiles.
- **Icy Satellite Interior Properties (I_AO4)** – Constrain models of the satellites' bulk compositions and internal structures.
- **Icy Satellite Magnetosphere and Ring Interactions (I_AO5)** – Investigate interactions with the magnetosphere and ring systems and possible gas injections into the magnetosphere.
- **Enceladus Seasonal Changes (IC1a)** – Identify long-term secular and seasonal changes at Enceladus, through observations of the south polar region, jets, and plumes.
- **Enceladus Ocean (IN1a)** – Determine the presence of an ocean at Enceladus as inferred from induced magnetic field and plume composition, search for possible anomalies in the internal structure of Enceladus as associated with plume sources, and constrain the mechanisms driving the endogenic activity by in situ observations and remote sensing.
- **Magnetosphere Wave-Particle Interactions (M_AO3)** – Investigate wave-particle interactions and dynamics of the dayside magnetosphere and the magnetotail of Saturn and their interactions with the solar wind, the satellites, and the rings.

- **Enceladus Plume Variability (MC1a)** – Determine the temporal variability of Enceladus' plumes.
- **Ionosphere and Ring Coupling (MN2a)** – Determine the coupling between Saturn's rings and ionosphere.
- **Ring Structure and Dynamics (R_AO1)** – Study configuration of the rings and dynamical processes (gravitational, viscous, erosional, and electromagnetic) responsible for ring structure.
- **Ring Particle Composition and Size (R_AO2)** – Map composition and size distribution of ring material.
- **Ring-Satellite Interaction (R_AO3)** – Investigate interrelation of rings and satellites, including embedded satellites.
- **Dust and Meteoroid Distribution (R_AO4)** – Determine dust and meteoroid distribution both in the vicinity of the rings and in interplanetary space.
- **Ring Magnetosphere-Ionosphere Interactions (R_AO5)** – Study interactions between the rings and Saturn's magnetosphere, ionosphere, and atmosphere.
- **Changing Rings (RC1a)** – Determine the seasonal variation of key ring properties and the microscale properties of ring structure, by observing at the seasonally maximum opening angle of the rings near solstice.
- **F-ring (RC2a)** – Focus on F-ring structure, and distribution of associated moonlets or clumps, as sparse observations show clumps, arcs, and possibly transient objects appearing and disappearing.
- **Ring Age and Origin (RN1a)** – Constrain the origin and age of the rings by direct determination of the ring mass, and of the composition of ring ejecta trapped on field lines.
- **Ring Composition (RN1b)** – Determine the composition of the close-in "ringmoons" as targets of opportunity.
- **Ring Structure (RN1c)** – Determine structural and compositional variations at high resolution across selected ring features of greatest interest, using remote and in situ observations.
- **Titan Upper Atmosphere (T_AO5)** – Investigate the upper atmosphere, its ionization, and its role as a source of neutral and ionized material for the magnetosphere of Saturn.

Table CDA-1. CDA Science Assessment: AO and TM objectives are paired with CDA science objectives.

Fully/Mostly Accomplished: **Partially Accomplished:**

CDA Science Objective	AO and TM Science Objective	CDA Ring Science Assessment	Comments if yellow (partly fulfilled)
Ring Science			
Structure and dynamics of E-ring	R_AO1, R_AO2, R_AO3, R_AO4, T_AO5, RN1c, RC1a		
Seasonal variation of E-ring	RC1a		Analysis is not complete.
Composition of E-ring	R_AO2, RN1b, RN1c		
E-ring origin	R_AO1, I_AO1, I_AO2, I_AO3, I_AO5, IN1a		
G-ring	R_AO1, RC2a		HRD was damaged by a grain larger than 100 microns during a near G-ring crossing in 2005.
Other diffuse rings / ring arcs	R_AO1, R_AO2, R_AO3		
In situ composition measurements of main ring material	R_AO1, R_AO2, RN1a		
Ring rain mass flux and structure	R_AO1, R_AO2, R_AO4, R_AO5, RN1a, MN2a		
Icy Satellites			
Enceladus			
Plume ice grain structure and size distribution	R_AO2, R_AO3, I_AO2, I_AO3, I_AO4, I_AO5, IC1a, IN1a, MC1a		
Plume ice grain mass output	R_AO3, I_AO4, IN1a		
Plume ice grain composition	I_AO1, I_AO4, IN1a		
Plume dynamics			
Ejecta from hypervelocity impacts on icy moons	R_AO1, R_AO2, R_AO3, R_AO4, I_AO5		Ring/ring arcs associated with moons were detected and studied. Despite multiple attempts, the existence of ejecta clouds around other mid-sized icy moons remains ambiguous because of the higher than expected E-ring background.
Magnetosphere			
E-ring grain charge	R_AO4, R_AO5, M_AO3		
Dynamics of Saturnian stream Particles	R_AO2, R_AO3, R_AO4, R_AO5, M_AO3		
Composition of Saturnian stream particles	R_AO2, R_AO3, R_AO5, M_AO3, I_AO1, I_AO4, IN1a		
Other (including cruise, Jupiter flyby)			
IDP (cruise)	C_AO4		
Exogenous mass infall	C_AO4, R_AO4, RN1a		
Interstellar dust	R_AO4		
Jovian nanograins (Jupiter flyby)	J_AO1		

CDA Saturn System Science Results

Rings

E-ring

Saturn's E-ring was one of the prime targets of CDA from the beginning of the mission. After the discovery of the plume activity on Enceladus and its recognition as the major source of the E-ring grains—see section entitled Enceladus and Spahn et al. [2006a]—the E-ring measurements became more important. Sampling the E-ring provides insights into not only the dynamical evolution of micron-sized grains but also the structure and composition of Enceladus' interior [Postberg et al. 2009b; Postberg et al. 2011]. In situ CDA measurements have characterized the E-ring spatial distribution, the grain size distribution, the electrostatic charge state, and the grain composition [Srama et al. 2006; Kempf et al. 2006, 2008a, 2010; McBride et al. 2007; Hillier et al. 2007a; Postberg et al. 2008; Ye et al. 2014, Hsu et al. 2015]. Both DA and HRD data have been used to derive the E-ring spatial distribution and the grain size distribution. The grain charge is measured by the entrance grid signal (QP) and the grain composition by the CA.

A side projection of the global apparent dust density is shown in Figure CDA-1. One has to keep in mind that the mass threshold during the related measurements was not fixed. The mass

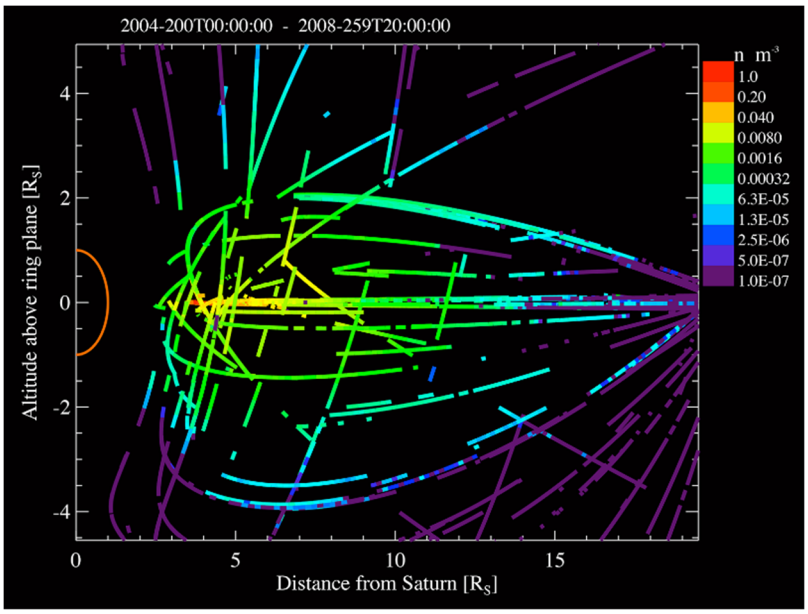

Figure CDA-1. Global apparent dust density measured by CDA in the Saturnian system. The densities are color coded along the Cassini trajectory in the time range of 2004-200 to 2008-259 (Cassini Prime Mission). High impact rates and densities are observed outside the optically measured E-ring, which was defined between 3 to 9 R_S. Enhanced dust densities are found as far as 250,000 km away from the ring plane and extend to radial distances of 20 R_S and beyond. From Srama et al. [2006].

threshold varied with relative impact speed and CDA becomes more sensitive for higher relative impact speeds. Assuming a typical relative impact speed of 8 km s^{-1}, the lower mass threshold would be 1.2×10^{-16} kg. This mass corresponds to compact water ice particles with a diameter of 0.6 µm.

Spatial Distribution

The densest part of the E-ring lies at ρ_c = 3.98 R_S (1 R_S is the radius of Saturn, 60,268 km), slightly outside the orbit of Enceladus (3.95 R_S) as known from pre-Cassini Earth-based observations [de Pater et al. 1996a]. The peak number density ranges from 16 to 21 × 10^{-2} m^{-3} for grains larger than 0.9 µm, and 2.1 to 7.6 × 10^{-2} m^{-3} for grains larger than 1.6 µm. The radial extension of the E-ring inferred from CDA measurements is much broader than that from the remote sensing observations. The E-ring encompasses all major icy moons of Saturn from 3 to 20 R_S [Srama et al. 2006, 2011], i.e., from the orbit of Mimas to that of Titan. The ring's vertical profiles are generally Gaussian, yet the vertical extension varies with the radial distance [Kempf et al. 2008b]. The narrowest part is located at ρ_c = 3.98 R_S with a full-width-half-maximum (FWHM) of 4,300 km. The vertical ring thickness increases both inwards and outwards from ρ_c. The density peak offsets towards the south with respect to the geometric ring plane at radial distances inside ρ_c. The offset is about 1,200 km at Mimas' orbit. No clear offset was found outside ρ_c in CDA data prior to 2008. An empirical, axisymmetric E-ring density model based on the CDA measurements is described in Kempf et al. [2008b].

The E-ring encompasses all major icy moons of Saturn from 3 to 20 R_S …, i.e., from the orbit of Mimas to that of Titan.

As reported by Hedman et al. [2012] based on imaging data, CDA measurements also indicate that the E-ring is asymmetric with respect to the local time [Kempf et al. 2012]. The data analysis and modeling efforts in understanding the day-night asymmetry of the E-ring are still ongoing.

Radial scans were performed by DA in the ring plane in order to determine the radial density profile of smaller grains (Figure CDA-2). As described earlier, the mass threshold was in the submicron range and variable. The density profile is compatible with a power law function of the type $n(r) = 20\ (r - 2.8)^{-4.6}$. This has to be considered a minimum density since particles below the detection threshold were not considered.

Grain Size Distribution

The grain size distribution of a diffuse ring sheds light on the grain production mechanism and the dynamical evolution of the ring. Under nominal encounter speeds in the E-ring, i.e., several km s^{-1}, DA was able to measure grains as small as 0.1 µm and HRD was sensitive to grain radii ranging from ~1 to 10 µm. The grain size distribution information is mostly derived from HRD because of the long dead time of the DA (~1 second)—see Kempf [2008b].

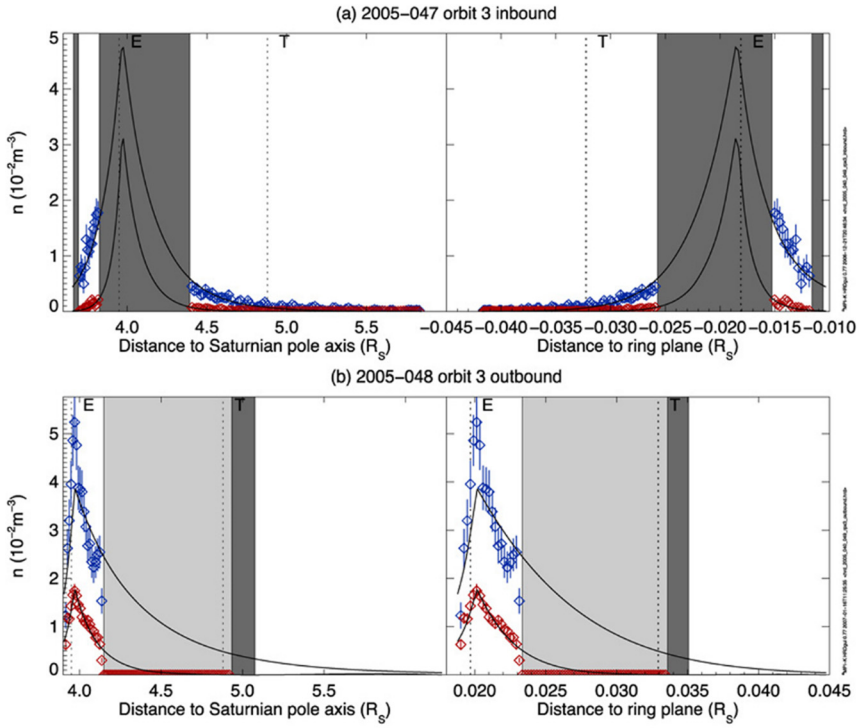

Figure CDA-2. E-ring number density profiles measured by CDA/HRD. Spatial distribution of E-ring particles 1.3 µm (red) and 2.4 µm inferred from HRD rate measurements inside 6 R_S in orbit 3. Solid curves are the empirical model given in Kempf et al. [2008b].

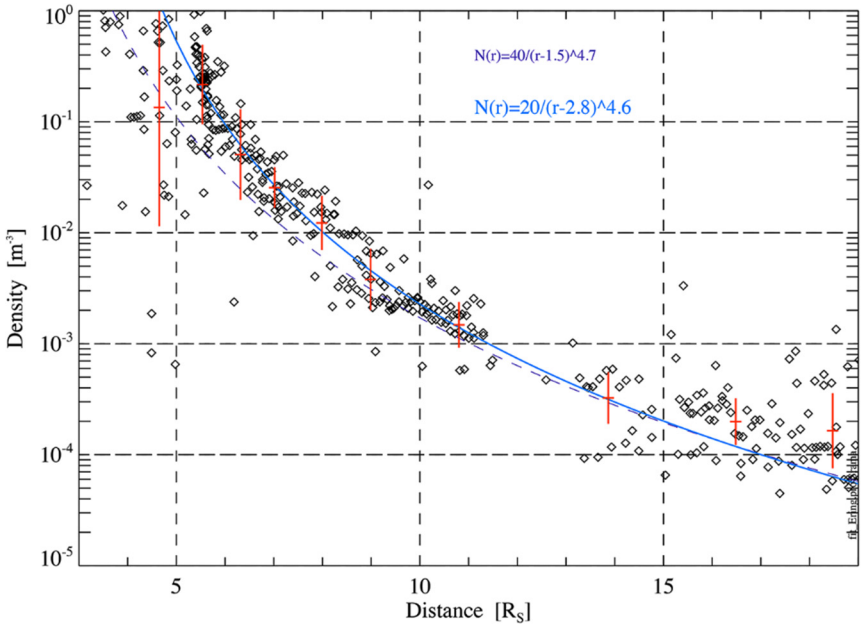

Figure CDA-3. Radial density profile of Saturn's E-ring measured in the ring plane. Data from the years between 2004 and 2008 were considered. Figure from [Srama et al. 2006].

The differential size distribution of E-ring grains is consistent with a power-law distribution, $n(s_d)\, ds_d \sim sd^{-q}\, ds_d$, with slope q = 4 to 5 for grains >0.9 μm [Kempf et al. 2008b]. s_d is the grain radius. The size slopes derived from the RPWS instrument are consistent within a range of q = 3 to 5 (Figure CDA-4) [Ye et al. 2014, 2016]. The steep size distribution slope is related to the E-ring's peculiar blue spectral color [Showalter et al. 1991; de Pater et al. 1996; Nicholson et al. 1996] and stems from the size-speed dependence of grains emitted from the plume of Enceladus (see section entitled Enceladus). In comparison, for diffuse rings supplied by ejecta from hypervelocity impacts on the source bodies, the size slopes are flatter (q ~ 2), resulting in a redder spectral color (e.g., G-ring, see section entitled Other Rings).

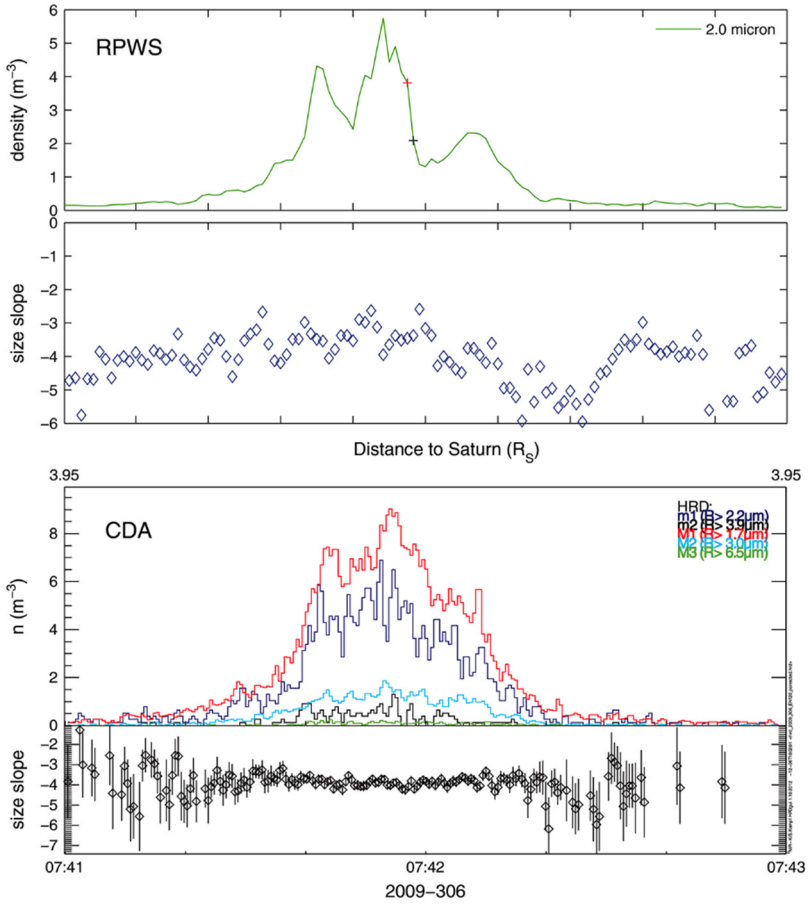

Figure CDA-4. Grain number density and the size distribution slope during E7 flyby by RPWS and CDA/HRD. Figure from Ye et al. [2014].

Grain Electrostatic Charge State

The Lorentz forces acting on a grain are determined by the number and the polarity of electric charges of a grain. The grain charge is determined by various charging processes, e.g., plasma electron and ion collections, photoemission and secondary electron emission, and thus is expected to vary with the magnetospheric plasma conditions [Horányi et al. 1992]. Figure CDA-5 shows the

CDA measurements of E-ring grain charges at various distances [Kempf et al. 2006]. Near Enceladus' orbit the grain potential is about −3 Volts, consistent with, but slightly lower than, the previous estimates based on Voyager plasma measurements [Horányi et al. 1992]. The grain potential becomes more positive with increasing distance and the polarity turns positive roughly outside the orbit of Rhea [Kempf et al. 2006] because of the decreasing plasma electron density and the increasing secondary electron emission resulting from the presence of more energetic electrons in the middle to outer magnetosphere [Arridge et al. 2011; Hsu et al. 2011b].

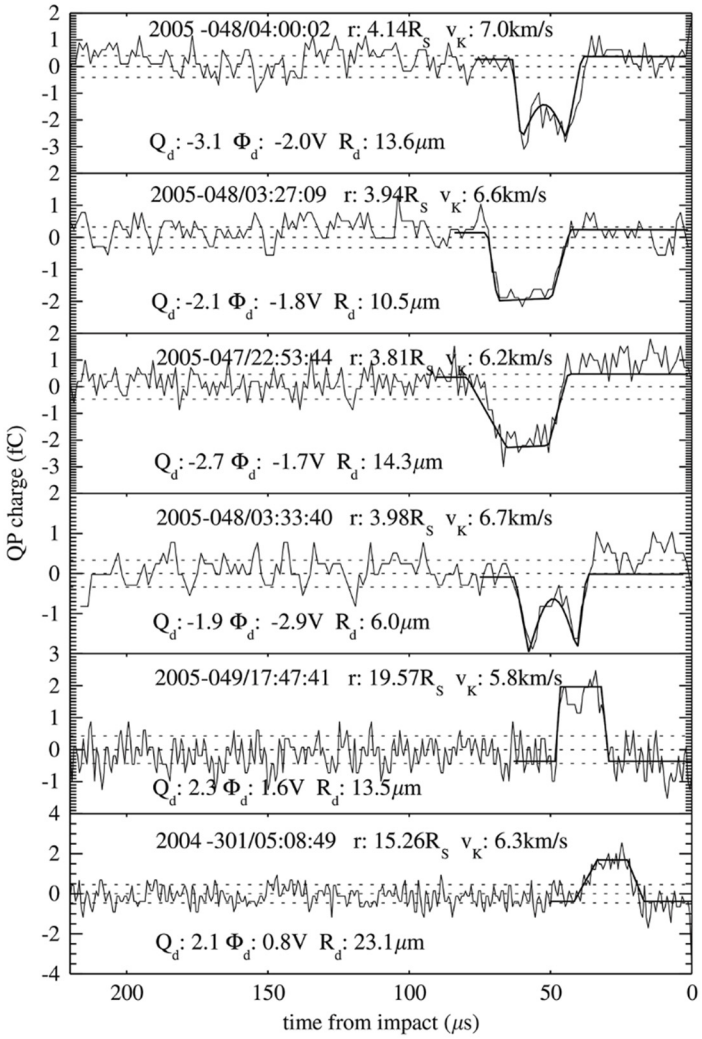

Figure CDA-5. Particle charge signals from the QP channel as measured by CDA in the E-ring at various radial distances from Saturn. The signal shape varies with particle speed (signal width), incident angle (signal asymmetry) and particle surface charge (signal amplitude). The signal sag is dependent upon the particle trajectory and its distance from the outer housing. From Kempf et al. [2006].

GRAIN COMPOSITION

E-ring grains are predominantly composed of water ice [McBride et al. 2007, Hillier et al. 2007a; Postberg et al. 2008]. The presence of minor grain constituents (up to a few percent levels), however, drastically changes mass spectral appearance because of the nature of impact ionization time-of-flight spectroscopy. Three major types of E-ring grain mass spectra have been identified (Figure CDA-6): Type I - pure water ice particles; Type II - water ice with organic compounds and/or silicate minerals impurities; and Type III - water ice rich in sodium salts [Postberg et al. 2008, 2009b, 2011]. The majority of the E-ring grains are either Type I or II, with only ~6% belonging to Type III.

The presence of Type III salty E-ring grains suggests the existence of subsurface liquid water underneath Enceladus' south polar terrain [Postberg et al. 2009b, 2011], in good agreement with the calculated thermodynamics result [Schmidt et al. 2008]. They are interpreted as frozen droplets lofted from liquid plume sources at the bottom of the fissures, representing direct samples of the subsurface waters within Enceladus [Postberg et al. 2009b, Postberg et al. 2011]. The salinity (0.5 to 2% by mass) and pH values (8 to 11) of the subsurface waters are also inferred [Postberg et al. 2009b]. Other findings about the icy moon Enceladus are addressed in the section entitled Enceladus.

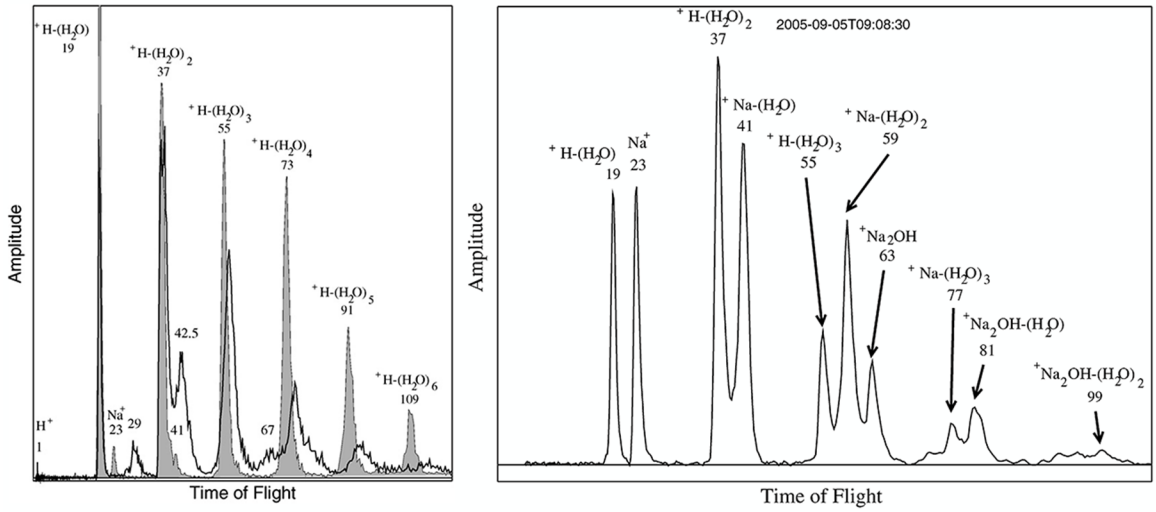

Figure CDA-6. Three major E-ring grain composition types. *Left*: Type I (pure water ice, gray) and Type II (water ice and organic compounds and/or silicate minerals, bright) E-ring grain mass spectra. The horizontal axis shows the cation time of flight. The vertical axis shows the peak amplitude. The Type I spectrum is characterized by the presence of water clusters, $H\text{-}(H_2O)^+_n$, where n = 1 to 6. Type II spectrum often show a wide feature at 42 to 43 u and 65 to 68 u. A shift of the water cluster peaks starts at n > 2 and increases towards longer times of flight. *Right*: Type III salt-rich E-ring grain mass spectrum. Water clusters ($H\text{-}(H_2O)^+_n$) seen in Type I spectrum are joined by sodium-water clusters, $Na\text{-}(H_2O)^+_n$ and $(Na_2OH)\text{-}(H_2O)^+_n$, because of the abundant Na^+. From Postberg et al. [2008].

GRAIN DYNAMICS MODELING

Joining pre-Cassini results, for example, Showalter et al. [1991]; de Pater et al. [1996]; Nicholson et al. [1996], the "ground truth" measurements provided by Cassini make Saturn's E-ring the most studied diffuse ring in the solar system. While the E-ring is particularly special because of its cryovolcanic origin, the same processes shaping the E-ring operate similarly elsewhere. Modeling efforts enable us to readily apply what has been learned from Saturn's E-ring to other environments.

> … Saturn's E-ring is the most studied diffuse ring in the solar system.

Regarding the E-ring dynamics, early modeling shows that the gravity from the oblate planet and the Lorentz forces from the electromagnetic fields lead to a size-dependent orbital precession rate ($\dot{\omega}$). For grains with radii around 1 μm, this leads to $\dot{\omega} \sim 0$ and allows a fast increase in the grains' orbital eccentricities by the solar radiation pressure force on timescales of a few years [Horányi et al. 1992; Hamilton 1993]. Additionally, the drag force asserted by the co-rotating magnetospheric plasma overtaking grains in semi-Keplerian orbits leads to an increase of the grains' orbital semi-major axes (i.e., grains gain orbital energy) [Dikarev 1999; Horányi et al. 2008]. Simultaneously, grain sizes are reduced by plasma sputtering erosion [Jurac et al. 2001; Juhasz and Horányi 2002; Horányi et al. 2008]. The combined effect of plasma drag and sputtering causes a reduction in grain sizes towards larger Saturn-centric distances without changing the size distribution [Horányi et al. 2008]. The radial extension of the E-ring up to Titan's orbit [Srama et al. 2006] also implies that Enceladus has been actively supplying the E-ring for at least hundreds of years.

Ejecta cloud and diffuse rings

In addition to the cryovolcanic E-ring, CDA also explored other diffuse rings, which are most likely supplied by impact ejecta produced from the embedded source bodies through continuous bombardment of micrometeoroids and the consequent fragmentation. Ejecta produced from airless bodies could appear in three forms, depending on the gravitational influences of the source body and its neighbors: a dust exosphere around the source body (e.g., around Galilean moons and Rhea), a complete ring (e.g., Saturn's G-ring), or a ring arc (a partial ring, e.g., the Anthe and Methone ring arcs). Modeling efforts provided theoretical support for characterizing the exogenous interplanetary mass infall [Han et al. 2011; Poppe and Horányi 2012] (see section entitled Interplanetary Dust) and the resulting ejecta cloud around major [Krivov et al. 2003; Sremčević et al. 2003; Dikarev et al. 2006; Spahn et al. 2006b] and minor [Sun et al. 2017] moons in the Saturnian system.

EJECTA CLOUD AROUND RHEA

In contrast to the clear detection of dust exospheres around Galilean moons [Krüger et al. 1999], the identification of such ejecta clouds around Saturn's major icy moons was ambiguous except at Rhea (8.75 R_S) [Jones et al. 2008], the major icy moon located furthest from the E-ring source

moon Enceladus (Figure CDA-7). Clearly, the background of the extensive E-ring renders a clear detection of a dust exosphere around the inner icy moons difficult.

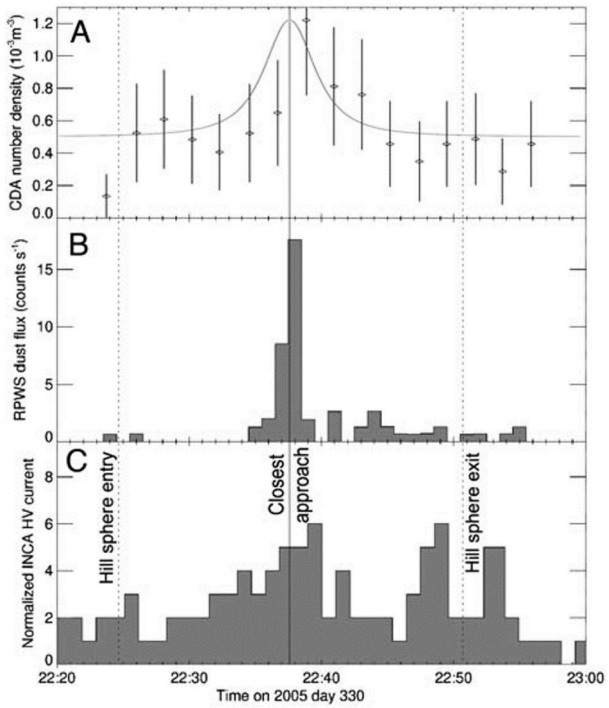

Figure CDA-7. In situ dust observations reveal the dust cloud around Rhea. Measurements from three in situ instruments during the Rhea flyby on November 26, 2005: (A) CDA (grains > 1 µm), (B) Radio and Plasma Wave Science instrument (grains ≥ 3 µm), and (C) Magnetosphere Imaging Instrument. From Jones et al. [2008].

Pallene ring

The dusty ring associated with a tiny moon, Pallene (mean radius ~2 km), at 3.52 R_S [Hedman et al. 2009b] has been detected by CDA/HRD in 2010 [Seiß et al. 2014]. The cross-section of the ring measured by HRD can be fitted with a double-Gaussian distribution, yielding a radial and vertical FWHM of 2,300 km and 270 km, respectively, and a maximum particle density of 2.7×10^{-3} m^{-3}. Additionally, the data clearly show an enhancement of larger particles in the Pallene ring compared to the background E-ring particles. In comparison, no in situ CDA detection of the ring arcs associated with Anthe (3.28 R_S) and Methone (3.23 R_S) has been reported so far.

G-ring

Collisions are expected to be the major dust production process that resupplies Saturn's G-ring, as indicated from its spectrally red color [de Pater et al. 1996; Nicholson et al. 1996]. However, no source was known prior to Cassini's arrival. The source of the G-ring was then identified, based on Cassini imaging data [Hedman et al. 2007], as a 60°-long arc. Collisional fragmentation of

centimeter- to meter-sized objects within this bright arc is believed to replenish the G-ring, which would otherwise disappear over relatively short timescales.

An impact of an exceptionally large dust grain (>100 μm) was registered and damaged HRD on September 5, 2005, when the spacecraft passed the ring plane at a radial distance of 2.93 R_S, less than 0.15 R_S from the core of the G-ring [Hedman et al. 2007]. The size of that grain is consistent with the impactor-ejecta production origin.

JANUS-EPIMETHEUS RING

During the ring grazing orbits, the spacecraft passed near the orbits of the co-orbital moons Janus and Epimetheus [Buratti et al. 2019]. A Gaussian distribution fit to the radial profile of grains larger than 1.6 μm registered by HRD show that the peak density is located very close to the orbits of Janus and Epimetheus at 151,500 km (2.51R_S) with a radial width of about 4,300 km.

Grand finale mission

The major science goals of CDA for the Grand Finale were: (1) perform in situ composition measurements of materials from the Main rings and (2) study the ring–planet interactions.

An analysis of CDA and RPWS measurements suggests that the region interior to Saturn's D-ring sampled during Cassini's Grand Finale Mission is predominantly populated by grains 10s of nm in radii, whose dynamics are consistent with high-speed impact ejecta from Saturn's main rings [Hsu et al. 2018]. Electromagnetic forces lead to the fast transport of tiny, charged ejecta grains (within hours, see Hsu et al. [2017]), which comprises a ring mass loss pathway (10^2 to 10^3 kg s^{-1}). About 20% of this ejecta falls into Saturn, mainly in the equatorial region and the southern hemisphere, leading to the observed H_3^+ ionospheric signature, i.e., the Ring Rain effect [O'Donoghue et al. 2013; Moore et al. 2015]. Two grain composition types were identified from ~25% of recorded mass spectra—water ice and silicates, with an ice fraction varying with the distance from the ring plane—decreasing from around 70–90% near the ring plane towards high latitudes. No indication of grains with pure organics, iron or iron-oxide compositions has been found in the dataset.

Icy Satellites

Enceladus

Ice grains emitted from Enceladus provide a unique window to probe the interior of Enceladus, as these tiny solid particles preserve information differently from that in gaseous and plasma phases. The micron-sized ice grains and the nanometer-sized silica stream particles probe the conditions of the subsurface water of Enceladus at different depths: the silica nanoparticles probe the pH, salinity and water temperature at the bottom of Enceladus' ocean, while the micrometer-sized ice

grains reveal composition and thermodynamical processes at near-surface liquid plume sources and in the vents.

Several sets of CDA measurements contribute to the study of Enceladus: (a) in the E-ring (described in the section entitled E-ring), (b) during the close Enceladus flybys, and (c) the Saturnian nanodust stream particles.

CLOSE ENCELADUS FLYBYS

Information provided by the CDA measurements during the plume crossings include the structure of the dusty plume (HRD) and the composition of freshly emitted grains (DA). The HRD data from the close encounter on July 14, 2005, showed that the grains in the vicinity of Enceladus are produced from a localized source near the south polar region [Spahn et al. 2006a], suggesting endogenic dust production at Enceladus as the major source of Saturn's diffuse E-ring. In addition, the structure of the plume provides constraints on the thermodynamics of the grains and vapor in the vents. The grain size distribution sampled by HRD is best explained by ice grain formation from condensation as water vapor reaches saturation when passing through the nozzles in the subsurface fissures (Figure CDA-8) [Schmidt et al. 2008]. A key characteristic successfully explained by this nozzle model is the size-dependent grain initial speeds, larger grains are emitted slower due to the longer time required to recover to the gas flow speed after a wall collision in the vent. This leads in a steepening of grain size distribution towards higher altitudes in the plume, consistent with measurements from the Visual and Infrared Imaging Spectrometer (VIMS) [Hedman et al. 2009a].

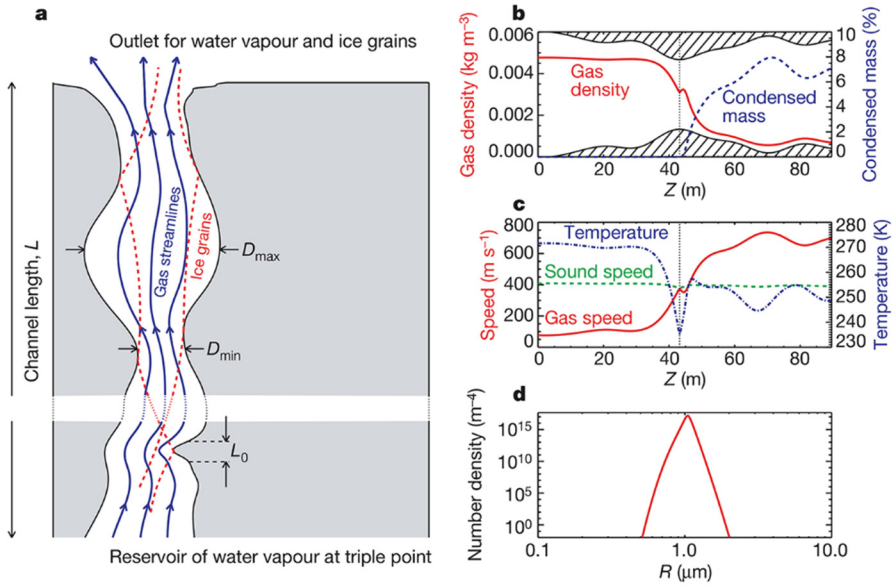

Figure CDA-8. The nozzle grain formation model. (a) Schematic sketch of the subsurface fissure profile describing the gas flow and ice grain condensation. (b, c) Thermodynamics conditions in the channel as a function of depth. (d) The resulting grain size distribution of one single channel. Figure from Schmidt et al. [2008].

Constrained by the HRD measurements, the mass production rate of micron-sized ice grains from the plume was estimated to be approximately 10 kg s^{-1} [Southworth et al. 2019], comparable with independent estimates from the imaging data [Ingersoll and Ewald 2011; Gao et al. 2016]. In addition, the deposition of plume ice grains onto Enceladus simulated with the same model shows a pattern resembling an infrared-ultraviolet brightness ratio map of Enceladus (Figure CDA-9) [Kempf et al. 2010; Schenk et al. 2011]. While this reinforces notions about the effects of the E-ring deposition and the surface albedo patterns of the major icy moons [Buratti et al. 1990; Verbiscer et al. 2007; Schenk et al. 2011], the detailed mechanisms remain unknown.

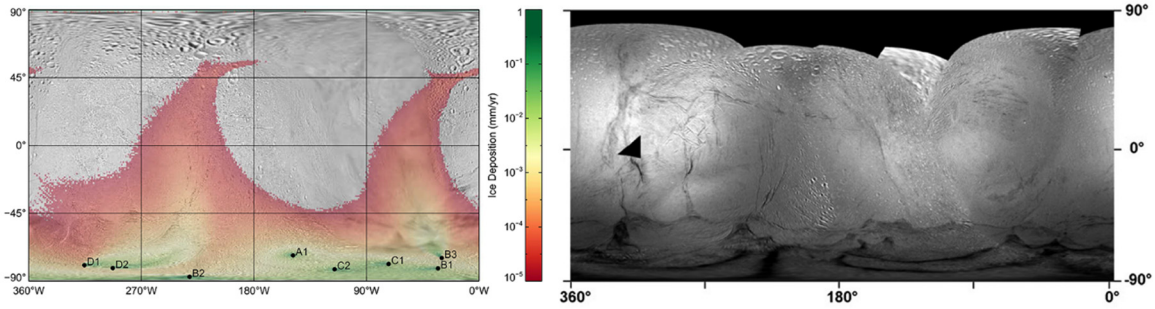

Figure CDA-9. Modeled plume deposition map (left) and the observed infrared/ultraviolet (IR/UV) ratio map of Enceladus (right). From Kempf et al. [2010] and Schenk et al. [2011].

Grain composition provides information about the subsurface waters of Enceladus. As mentioned, the presence of Type III (salt-rich) E-ring grains indicates salty, alkaline subsurface waters within Enceladus [Postberg et al. 2009b]. The grain composition profile recorded during the E5 close encounter in 2008 shows that the ratio of Type III grains increases from the E-ring background of around 6% to 40% at the closest approach (altitude of 25 km) [Postberg et al. 2011]. A clear decrease of the proportion of Type I grains in the dense plume region was confirmed by data of the E17 flyby in 2012 [Khawaja et al. 2017]. The dominance of the larger, salty ice grains at lower altitudes indicates a stratified plume [Hedman et al. 2009a; Postberg et al. 2011] and is consistent with the aforementioned modeling results [Schmidt et al. 2008]. In other words, the grain composition stratification reflects the grain formation processes in the fissures (Figure CDA-10) and thus strongly suggests that subsurface waters are the direct source of the plume [Postberg et al. 2011]. This result also agrees with the low abundance of salty ice grain (Type III) in the E-ring [Postberg et al. 2008]—most grains capable of escaping Enceladus to resupply the E-ring are smaller, and therefore faster, pure ice grains forming from condensation in the vents. Salty grains tend to be heavier/slower and mostly fall back onto the moon [Kempf et al. 2010; Postberg et al. 2011].

A subset of E-ring Type II spectra was found to contain a series of mass lines indicating the presence of complex organic molecules with a mass fraction of about 1% of the ice grain [Postberg et al. 2018]. As shown in Figure CDA-11, the species marked high mass organic cation (HMOC) show regular ~12.5 u separation and extend to beyond ~200 u mass range, indicating that they are fragments of larger parent molecules whose mass may be in the 1,000s u region. The observation suggests the existence of a thin film at the subsurface water liquid-vapor interface composed of complex organics likely originating from hydrothermal activities deep inside Enceladus.

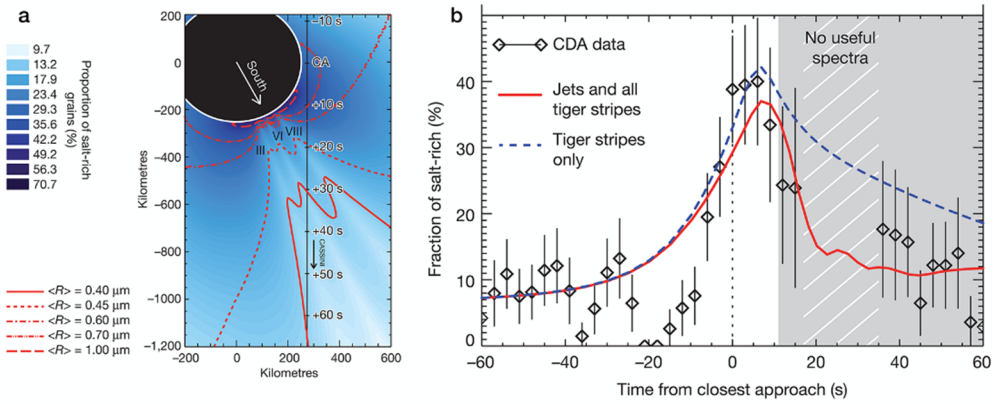

Figure CDA-10. Compositional and size profile of the ice plume of Enceladus. (a) The background color and the contour lines show the modeled fraction of salt-rich grains and the mean particle radius <*R*> of grains emitted from the plume of Enceladus. (b) Measured Type III spectrum fraction as a function of time during the E5 Enceladus flyby. Model and measurement results consistently show that the closer to the surface, the higher the fraction of Type III ice grains. Figure from Postberg et al. [2011].

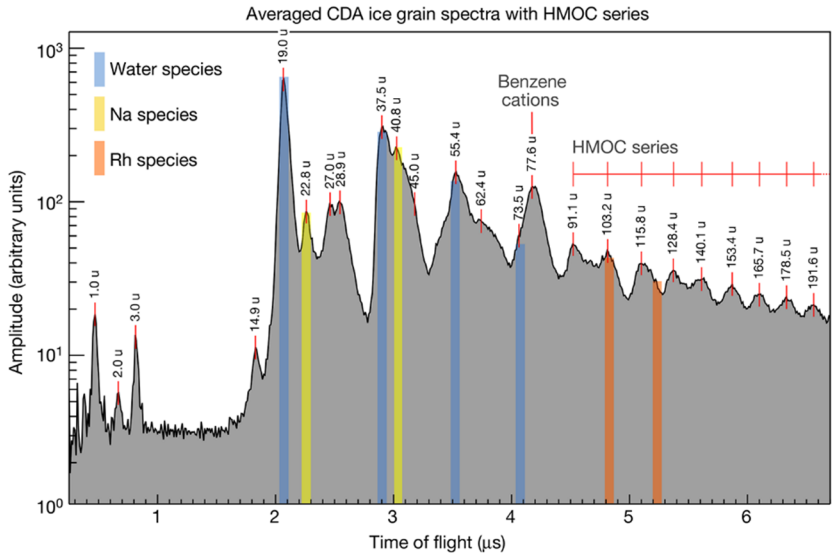

Figure CDA-11. CDA HMOC spectrum. This spectrum is co-added from 64 Type II E-ring spectra containing complex organic features. Benzene-like cations (77.6 u) and their fragments (C2 to C4 species) as well as the (HMOC, 91 u, and higher) appear distinctively from water (blue) and CDA target (Rh, orange) and target contamination (Na, yellow) mass lines. Figure from Postberg et al. [2018].

NANO-PHASE SILICA PARTICLES

The fast, nanometer-scale silicon-rich grains emitted into interplanetary space from the Saturnian system were the first CDA discovery [Kempf et al. 2005a, 2005b], despite the theoretical prediction [Horányi 2000] based on the knowledge of their Jovian counterparts [Grün et al. 1993]. These nanoparticles are in fact the silicon fingerprint of the ongoing hydrothermal activities within Enceladus [Hsu et al. 2015; Sekine et al. 2015].

Since the dynamical properties of the nanograins are beyond the CDA calibrated range, their sizes (2 to 8 nm) and ejection speeds (50 to 200 km s^{-1}) are derived based on the interactions with the IMF [Hsu et al. 2010a, 2010b, 2011a, 2011b, 2012b]. These grains are interpreted to be of Enceladus origin—they are erosion-resistant impurities embedded in micron-sized E-ring grains, which are released after the surrounding ice matrix is removed by the plasma sputtering erosion [Hsu et al. 2011b].

One surprising factor regarding their composition is their extremely low metal concentration. Detailed analysis, including the laboratory hydrothermal reaction experiments, show that these grains are nanometer-sized metal-free silicon-oxide, i.e., nano-phase silica (SiO_2, Figure CDA-12b), which is best explained as nm-sized colloidal silica stemming from hydrothermal interactions within Enceladus [Hsu et al. 2015; Sekine et al. 2015]. The instability of the nano-phase silica sets strong constraints on the internal conditions of Enceladus subsurface waters (see Figure CDA-13), including (a) a water-rock reaction temperature of >90°C; (b) a low salinity ocean region (<4%) and an alkaline pH value (8.5 to 10.5), in good agreement with [Postberg et al. 2009b]; (c) Enceladus' rocky core is likely undifferentiated and porous, with a primordial composition similar to carbonaceous chondrites;

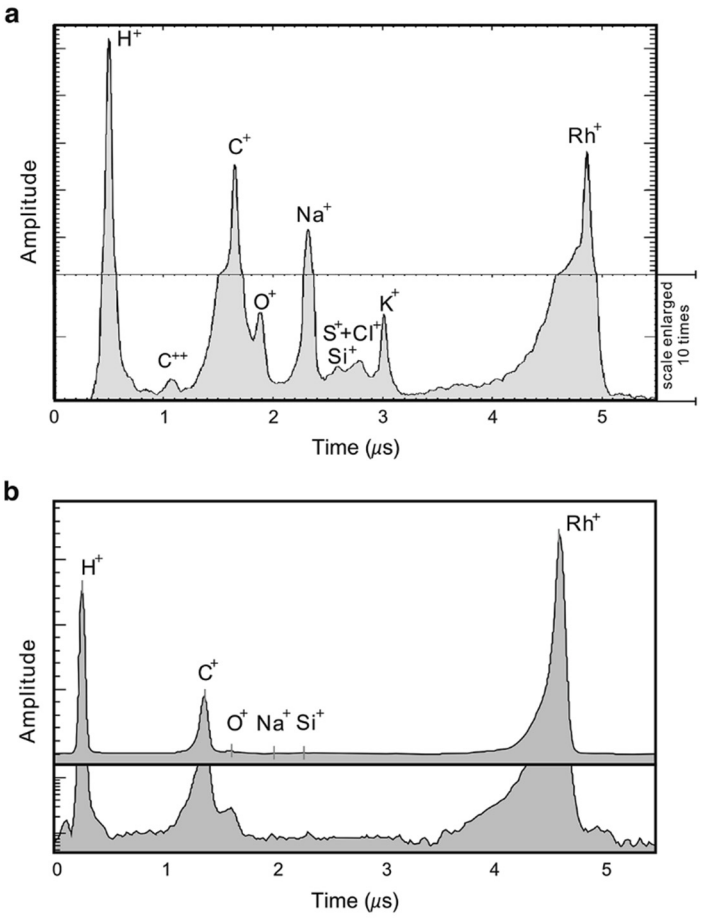

Figure CDA-12. CDA mass spectra of Jovian (*a*) and Saturnian (b) stream particles. Figure from Hsu et al. [2012b].

and (d) fast vertical transportation of the hydrothermal fluid from Enceladus' subsurface ocean to the plume within several years [Hsu et al. 2015; Sekine et al. 2015].

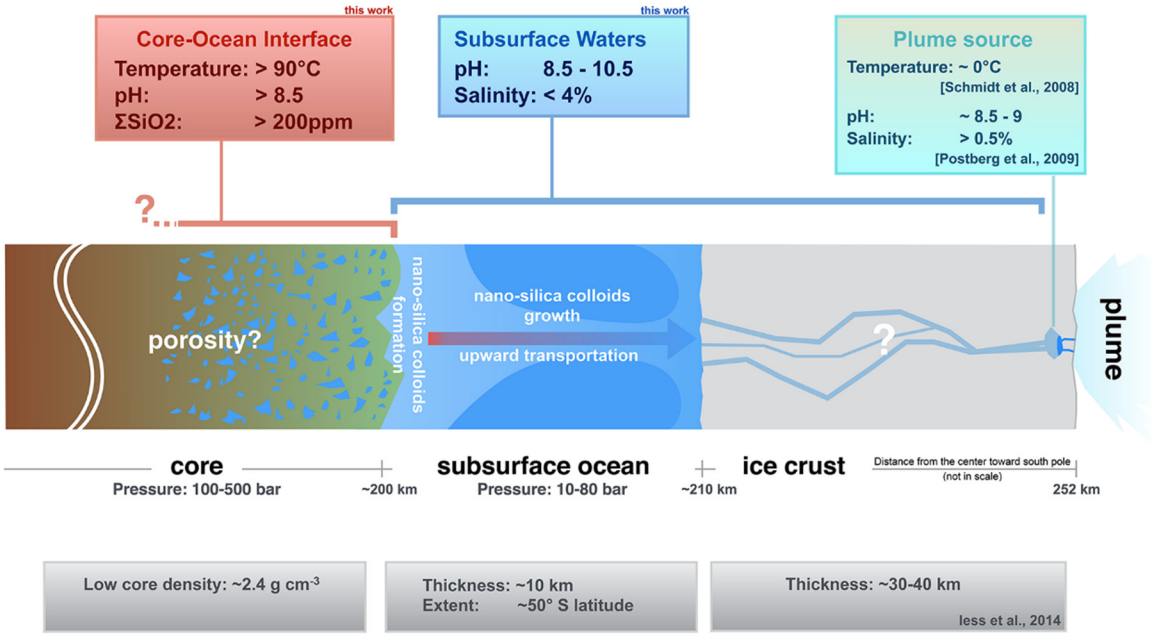

Figure CDA-13. A schematic of Enceladus' interior derived from the nano-phase silica results. Figure from Hsu et al. [2015].

Ejecta from Saturn's moons

As discussed in the section entitled Other Rings, the only major moon of Saturn around which an ejecta cloud was detected is Rhea [Jones et al. 2008]. The dusty rings associated with Pallene [Seiß et al. 2014], and Janus and Epimetheus [Buratti et al. 2019] were also explored in situ by CDA.

Magnetospheric and Plasma Science

Dust-magnetospheric plasma interactions

Grain charging, plasma sputtering, and plasma drag force

Magnetospheric plasma influences the charging, erosion, and dynamical processes of circumplanetary dust populations. In addition to the grain charge measurements in Saturn's E-ring [Kempf et al. 2006], as described in the section entitled E-ring, in situ E-ring characterization by CDA also provides constraints on the effects of the plasma sputtering erosion and the drag force. As illustrated in the modeling work by [Horányi et al. 2008], due to the plasma drag, grains from Enceladus can be transported from 4 to 20 R_S, and will arrive there with a few percentage of their

original radius due to sputtering losses, consistent with CDA measurements [Srama et al. 2006, 2011]. These calculations also indicate that the geysers on Enceladus have been supplying the E-ring material at an approximately constant rate for at least the last 300 years [Horányi et al. 2008].

Spacecraft charging

Strong interferences caused by dust impacts during the crossings of Enceladus' dusty plume have been reported from several instrument teams [Morooka et al. 2011; Ye et al. 2014; Krupp et al. 2018], likely caused by impact plasma produced from intense dust-spacecraft impacts. Because of the low plasma temperature of such an impact plasma cloud (~1 eV), this impact-generated plasma cloud may act as a buffer that reduces the spacecraft potential when traversing through a dust-rich region at high speed. The proposed effect has been examined by comparing the modeled spacecraft potential based on the CDA measurements to the Langmuir probe results during the plume and E-ring crossings [Hsu et al. 2012a, 2013a].

Nanodust dynamics in interplanetary space

CDA measurements also reveal the dynamical interactions of the Saturnian stream particles with the interplanetary magnetic field. After entering interplanetary space, the dynamics of the charged nanodust is governed by the IMF. CDA observed an identical detection pattern when the spacecraft crossed two similar solar wind compression regions associated with the Corotation Interaction Region (CIR), during the declining phase of solar activity in 2004 [Hsu et al. 2010b, 2011a]. These measurements illustrate that the nature of the dust stream phenomenon, first discovered by the Ulysses at Jupiter [Grün et al. 1993], is not in a form of collimated beams but a gust of electromagnetic acceleration of charged nanodust within a thick, warped dust sheet extending up to several astronomical units (AUs) from the source planets [Hsu et al. 2010a, 2010b].

Solar wind-magnetosphere interactions

The nanodust stream particle dataset is also relevant for studying the solar wind-magnetosphere interactions at Saturn. Serendipitous detections of a recurring pattern consisting of energetic stream particles coming from oblique directions are interpreted as the reentry of emitted stream particles back into their source magnetosphere due to the interaction with IMF [Hsu et al. 2013b]. Numerical simulation results show that this is simply due to the pick-up of the charged nanodust by the solar wind. The returning nanograins acquired kinetic energies higher than their initial kinetic energies gained from the magnetosphere, by being picked up in the compressed, high magnetic field strength solar wind regions. This means that this population can be easily identified and, more importantly, their directionality reflects the tangential component of the IMF. The latter provides additional information about the sector structure of the solar wind at Saturn's location. In other words, these measurements demonstrate an alternative method by which a single spacecraft can probe the solar wind conditions from within the magnetosphere [Hsu et al. 2013b; Hsu et al. 2016].

Instrument

In addition to the description of the CDA instrument [Srama et al. 2004], two publications provide information relevant for the CDA data analysis: (a) the DA dead time correction [Kempf 2008b] and (b) the contamination of the rhodium target of the integrated time-of-flight mass spectrometer [Postberg et al. 2009a].

Non-Saturn Science Results

Jovian Nanodust Stream Particles

"Ashes" from the volcanic plumes of Io, having acquired sufficient electric charges, may be accelerated by Jupiter's powerful magnetosphere and ejected with speeds comparable to the solar wind [Horányi et al. 1993; Graps et al. 2000]. These so-called stream particles were discovered during the first Ulysses flyby of Jupiter in 1992 by the onboard dust detector [Grün et al. 1993]. The detection patterns as registered by the Galileo Dust Detection System [Grün et al. 1992] suggest that they are modulated by the structure of the Io plasma torus (IPT) [Krüger et al. 2003b] as well as the temporal variation of Io's volcanic activities [Krüger et al. 2003a]. The stream could be detected by Galileo and Ulysses many 100 Mkm away from Jupiter.

Cassini CDA performed the first composition measurement of the Jovian stream particles before and after its Jupiter flyby in 2000/2001.

Cassini CDA performed the first composition measurement of the Jovian stream particles before and after its Jupiter flyby in 2000/2001 [Postberg et al. 2006]. Figure CDA-14 shows that these ash particles are mainly composed of sodium chloride (NaCl). In contrast to the sulfur-rich environment of Io, sulfur or sulfurous components and potassium-bearing components are only identified as minor constituents. Trace amounts of silicates or rocky minerals are often found. It is suggested that sodium chloride particles are formed inside Pele-type plumes prior to the condensation of the volatile SO_2. The less refractory sulfur compounds, in particular SO_2, either do not condense abundantly onto the grains, or are lost in bow shock regions at the top of the plumes, before the grains acquire sufficient electric charges to escape into Io's exosphere [Postberg et al. 2006]. The proposed scenario is in good agreement with the New Horizons observation of plume particle condensation in the eruption of Tvashtar [Spencer et al. 2007].

The CDA measurements of Jovian stream particles lasted about 10 months, roughly from day of year (DOY) 240 of 2000 to DOY 170 of 2001. A qualitative analysis of the CDA impact rate shows a correlation with the Galileo measurements [Hsu et al. 2010a, 2012b; Krüger et al. 2003b], reinforcing the idea of using Jovian stream particles as a monitor of Io's volcanic activities [Krüger et al. 2003a].

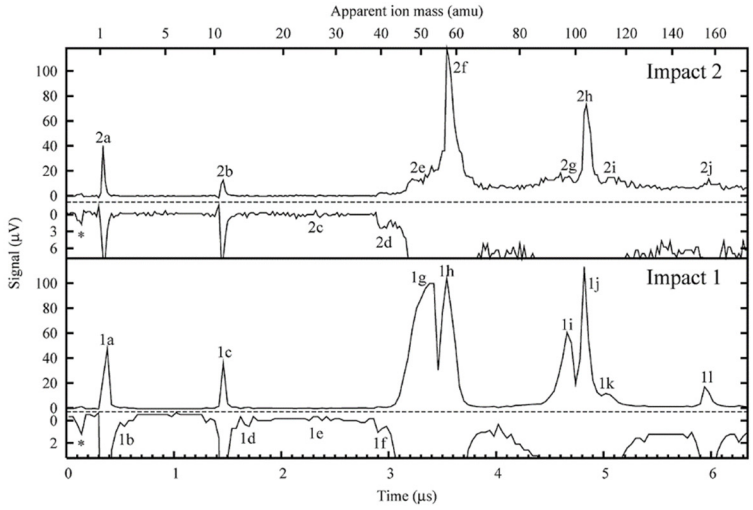

Ion abundances for both impacts

Species (key in Fig. 1)	Time (μs)	$\int Q_M$	Ions
Impact 1			
H^+ (1a), H_2^+ (1b)	0.28–0.64	2.71×10^{-12}	52,200
C^+ (1c)	1.36–1.58	2.22×10^{-12}	42,800
O^+ (1d)	1.6–1.72	3.16×10^{-14}	600
K^+ (1f)	2.84–2.96	1.09×10^{-13}	2100
'Fast Fe^+' (1g)	2.96–3.44	2.61×10^{-11}	503,300
'Slow Fe^+' (1h)	3.44–3.84	1.24×10^{-11}	239,300
'Fast Rh^+' (1i)	4.00–4.72	1.06×10^{-11}	204,200
'Slow Rh^+' (1j)	4.72–4.96	9.92×10^{-12}	191,400
RhC^+/Fe_2^+ (1k)	4.96–5.20	1.92×10^{-12}	37,000
$RhFe^+$ (1l)	5.80–6.12	1.77×10^{-12}	34,100
Total			1,307,000
Impact 2			
H^+ (2a)	0.3–0.42	1.25×10^{-12}	44,700
C^+ (2b)	1.42–1.58	5.41×10^{-13}	19,300
K^+ (2d)	2.88-3.02	2.99×10^{-13}	10,700
'Fast Fe^+' (2e)	3.02–3.46	5.25×10^{-12}	187,400
'Slow Fe^+' (2f)	3.46–3.88	1.56×10^{-11}	557,800
'Fast Rh^+' (2g)	4.16–4.74	6.67×10^{-12}	238,100
'Slow Rh^+' (2h)	4.74–4.98	7.72×10^{-12}	275,600
RhC^+/Fe_2^+ (2i)	4.98–5.22	2.96×10^{-12}	105,600
$RhFe^+$ (2j)	5.88–6.12	2.10×10^{-12}	74,900
Total			1,514,100

Figure CDA-14. CDA IDP TOF mass spectra detected during the cruise phase. *Left*: The time-of-flight mass spectra of two interplanetary dust particles detected in 1999. *Right*: The table shows the identified cation of each corresponding mass peak. From Hillier et al. [2007b].

Interplanetary Dust

Cruise phase

The interplanetary dust environment in between the orbits of Earth and Jupiter was explored during the cruise phase, during 1999 to early 2000 when the spacecraft was around 1 to 2.5 AUs away from the Sun [Kempf et al. 2004; Hillier et al. 2007b]. The detections of bound IDPs and unbound ISD in between the Jupiter flyby (2000-365) and the Saturn Orbit Insertion (SOI, 2004-183) are reported by Altobelli et al. [2007a, 2007b]. While the CDA dataset is limited by the spacecraft pointing, the CDA IDP measurements are in general consistent with the Pioneer results from the 70s. However, due to spacecraft activities no dust measurements were possible during the asteroid belt crossing.

Two mass spectra of IDPs were registered on 1999-147 and 1999-314, at heliospheric distances of 0.89 and 1.87 AU, respectively. These grains are roughly 2 μm in radii and both have an iron-rich composition [Hillier et al. 2007b]. Surprisingly, silicates and magnesium do not feature predominantly in the spectra. They are likely to have originated from near-Earth asteroid families (Aten and Apollo family, respectively), or Jupiter-family comets.

Kempf et al. [2004] reported in total 37 registered IDP impacts between November 1999 and January 2000. Among them, 6 impacts were obtained whose QP signals identified show a clear feature caused by charged grains, corresponding to Q_d between 1.3 and 5.4 fC [Auer et al. 2002; Kempf et al. 2004]. Assuming a potential of $\varphi_d \approx +5$ V and spheroidal grain morphologies, the corresponding grain masses are found to be in excess of 10^{-13} kg. The detection rate reasonably matches the IDP flux prediction [Staubach et al. 1997].

Between the Jupiter flyby and SOI, 7 of the total of 17 impact events were identified as IDPs based on their directionality [Altobelli et al. 2007a, 2007b]. These grains show a large spread in mass, ranging from 2×10^{-16} to 10^{-11} kg, corresponding to grain radii of 3 to 11 μm assuming a bulk grain density of 2 kg m^{-3}. These grains are most likely in orbits with low inclination and low eccentricity and likely originate from the short-period external Jupiter family comets and Edgeworth-Kuiper Belt objects [Altobelli et al. 2007b].

Exogenous mass infall at Saturn

Grains migrating inwards from the Edgeworth-Kuiper belt are expected to be an important exogenous dust population entering the Saturnian system [Han et al. 2011; Poppe and Horányi 2012]. Recent modeling results suggest grains approach Saturn's Hill sphere with speeds lower than expected (<3 km s^{-1}), meaning that the IDP flux enhancement by the gravitational focusing of Saturn is significant and the exogenous flux highly depends on the location of the moons/rings [Poppe and Horányi 2012].

Interstellar Dust

ISD is the major ingredient in planetary formation. The flow of these charged grains is mainly shaped by the solar radiation pressure force and the IMF configuration [Grün et al. 2000; Sterken et al. 2012]. The interplanetary cruise of Cassini during the first half of year 1999 provided an ideal window to monitor these interstellar messengers as the spacecraft traveled upstream with respect to the ISD flow [Altobelli et al. 2003]. The mean interstellar flux measured during this period of time, corresponding to heliospheric distances between 0.7 and 1.2 AU, is $2.5 \pm 0.5 \times 10^{-5}$ m^{-2} s^{-1}, in the grain mass range of $5 \times 10e^{-17}$ kg to 10^{-15} kg [Altobelli et al. 2003], in good agreement with the ISD flux measured by Ulysses at 3 AU during the same time period [Landgraf et al. 2003]. These simultaneous measurements demonstrate that relatively large interstellar grains (radii > 0.4 μm) can penetrate deeply into the inner solar system.

At 5 to 9 AU from the Sun, corresponding to the time in between the Jupiter flyby and SOI, 6 out of the 17 events registered are consistent with interstellar origin [Altobelli et al. 2007b]. The grain sizes are around 0.4 μm and the upper limit value of the flux is estimated to be 2×10^{-5} m^{-2} s^{-1}, consistent with the previous results.

ISD composition has been studied based on measurements at Saturn during 2004 to 2013 [Altobelli et al. 2016]. The mass distribution of 36 interstellar grains, their elemental composition, and a lower limit for the ISD flux at Saturn were determined [Altobelli et al. 2016]. Mass spectra and grain dynamics suggest the presence of magnesium-rich grains of silicate and oxide composition, partly with iron inclusions. Major rock-forming elements (magnesium, silicon, iron, and calcium) are present in cosmic abundances, with only small grain-to-grain variations, but sulfur and carbon are depleted. The ISD grains in the solar neighborhood appear to be homogenized, likely by repeated processing in the interstellar medium (Figure CDA-15).

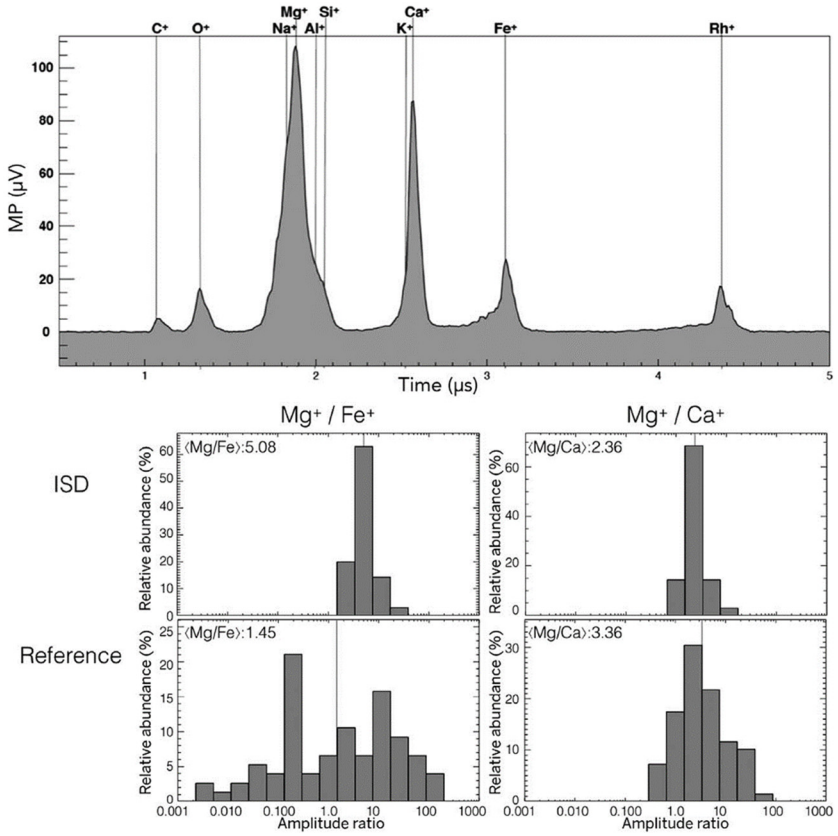

Figure CDA-15. Typical CDA ISD TOF mass spectrum and spectra comparison. *Top*: An example CDA time-of-flight mass spectrum of an ISD grain. *Bottom*: The comparison of cations from ISD spectra to that from the reference group spectra shows that ISD grains have a similar composition. From Altobelli et al. [2016].

ACRONYMS

Note: For a complete list of Acronyms, refer to Cassini Acronyms – Attachment A.

AO	Announcement of Opportunity
AU	astronomical unit
CA	chemical analyzer
CDA	cosmic dust analyzer
CIR	Corotation Interaction Region
DA	dust analyzer
DOY	day of year
FWHM	full-width-half-maximum
HMOC	high mass organic cation
HRD	high-rate detector
IDP	interplanetary dust particle
IID	impact ionization detector
IMF	interplanetary magnetic field
IPT	Io Plasma Torus
IR/UV	infrared/ultraviolet
ISD	interstellar dust
NaCl	sodium chloride
PVDF	polyvinylidene fluoride
RPWS	Radio and Plasma Wave Science
SOI	Saturn Orbit Insertion
TM	Traceability Matrix
TOF MS	time-of-flight mass spectrometry
VIMS	Visual and Infrared Imaging Spectrometer

REFERENCES

Disclaimer: The partial list of references below correspond with in-text references indicated in this report. For all other Cassini references, refer to Attachment B – References & Bibliographies; Attachment C – Cassini Science Bibliographies; the sections entitled References contributed by individual Cassini instrument and discipline teams located in Volume 1 Sections 3.1 and 3.2 Science Results; and other resources outside of the Cassini Final Mission Report.

Altobelli, N., F. Postberg, K. Fiege, M. Trieloff, H. Kimura, V. J. Sterken, H.-W. Hsu, J. Hillier, N. Khawaja, G. Moragas-Klostermeyer, J. Blum, M. Burton, R. Srama, S. Kempf, E. Grün, (2016), Flux and composition of interstellar dust at Saturn from Cassini's Cosmic Dust Analyzer, Science, 352, 312–318.

Altobelli, N., V. Dikarev, S. Kempf, R. Srama, S. Helfert, G. Moragas-Klostermeyer, M. Roy, E. Grün, (2007a), Cassini/Cosmic Dust Analyzer in situ dust measurements between Jupiter and Saturn, Journal of Geophysical Research, 112(A11), 7105.

Altobelli, N., S. Kempf, M. Roy, R. Srama, S. Helfert, G. Moragas-Klostermeyer, E. Grün, (2007b), Preliminary results on analysis of the Cosmic Dust Analyzer data between Jupiter and Saturn, Dust in Planetary Systems, 643, 65–68.

Altobelli, N., S. Kempf, M. Landgraf, R. Srama, V. Dikarev, H. Krüger, G. Moragas-Klostermeyer, G., E. Grün, (2003), Cassini between Venus and Earth, Detection of interstellar grains, Journal of Geophysical Research, 108(A10), 7–1.

Arridge, C. S., N. André, H. J. McAndrews, E. J. Bunce, M. H. Burger, K. C. Hansen, H.-W. Hsu, R. E. Johnson, G. H. Jones, S. Kempf, K. K. Khurana, N. Krupp, W. S. Kurth, J. S. Leisner, C. Paranicas, E. Roussos, C. T. Russell, P. Schippers, E. C. Sittler, H. T. Smith, M. F. Thomsen, M. K. Dougherty, (2011), Mapping magnetospheric equatorial regions at Saturn from Cassini Prime Mission observations, Space Science Reviews, 164, 1–83.

Auer, S., E. Grün, R. Srama, S. Kempf, R. Auer, (2002), The charge and velocity detector of the Cosmic Dust Analyzer on Cassini, Planetary and Space Science, 50, 773–779.

Buratti, B. J., P. C. Thomas, E. Roussos, C. Howett, M. Seiß, A. R. Hendrix, P. Helfenstein, R. H. Brown, R. N. Clark, T. Denk, G. Filacchione, H. Hoffmann, G. H. Jones, N. Khawaja, P. Kollmann, N. Krupp, J. Lunine, T. W. Momary, C. Paranicas, F. Postberg, M. Sachse, F. Spahn, J. Spencer, R. Srama, T. Albin, K. H. Baines, M. Ciarniello, T. Economou, H.-W. Hsu, S. Kempf, S. M. Krimigis, D. Mitchell, G. Moragas-Klostermeyer, P. D. Nicholson, C. C. Porco, H. Rosenberg, J. Simolka, L. A. Soderblom (2019), Close Cassini flybys of Saturn's ring moons Pan, Daphnis, Atlas, Pandora, and Epimetheus, Science, 364(6445), eaat2349, doi: 10.1126/science.aat2349.

Buratti, B. J., J. A. Mosher, J. A., T.V. Johnson, (1990), Albedo and color maps of the Saturnian satellites, Icarus, 87, 339–357.

de Pater, I., M. R. Showalter, J. J. Lissauer, J. R. Graham, (1996), Keck infrared observations of Saturn's E and G rings during Earth's 1995 ring plane crossings, Icarus, 121, 195–198.

Dikarev, V. V., A. V. Krivov, E. Grün, (2006), Two stages of dust delivery from satellites to planetary rings, Planetary and Space Science, 54, 1014–1023.

Dikarev, V., (1999), Dynamics of particles in Saturn's E ring, effects of charge variations and the plasma drag force, Astronomy and Astrophysics, 346, 1011–1019.

Gao, P., P. Kopparla, X. Zhang, A. P. Ingersoll, (2016), Aggregate particles in the plumes of Enceladus, Icarus, 264, 227–238.

Graps, A., E. Grün, H. Svedhem, H. Krüger, M. Horányi, A. Heck, S. Lammers, (2000), Io as a source of the Jovian dust streams, Nature, 405, 48–50.

Grün, E., M. Landgraf, M. Horányi, J. Kissel, H. Krüger, R. Srama, H. Svedhem, P. Withnell, (2000), Techniques for galactic dust measurements in the heliosphere, Journal of Geophysical Research, 105, 10403–10410.

Grün, E., H. Zook, M. Baguhl, A. Balogh, S. Bame, H. Fechtig, R. Forsyth, M. Hanner, M. Horányi, J. Kissel, B.-A. Lindblad, D. Linkert, G. Linkert, I. Mann, J. McDonnel, G. Morfill, J. Phillips, C. Polanskey, G. Schwehm, N. Siddique, P. Staubach, J. Svestka, A. Taylor, (1993), Discovery of Jovian dust streams and interstellar grains by the Ulysses spacecraft, Nature, 362, 428–430.

Grün, E., H. Fechtig, M. S. Hanner, J. Kissel, B.-A. Lindblad, D. Linkert, D. Maas, G. E. Morfill, H. A. Zook, (1992), The Galileo Dust Detector, Space Science Reviews, 60, 317–340.

Hamilton, D. P., (1993), Motion of dust in a planetary magnetosphere - orbit-averaged equations for oblateness, electromagnetic, and radiation forces with application to Saturn's E ring, Icarus, 101, 244–264.

Han, D., A. R. Poppe, M. Piquette, E. Grün, M. Horányi, (2011), Constraints on dust production in the Edgeworth-Kuiper Belt from Pioneer 10 and New Horizons measurements, Geophysical Research Letters, 38, L24102.

Hedman, M. M., J. A. Burns, D. P. Hamilton, M. R. Showalter, (2012), The three-dimensional structure of Saturn's E ring, Icarus, 217, 322–338.

Hedman, M. M., C. D. Murray, N. J. Cooper, M. S. Tiscareno, K. Beurle, M. W. Evans, J. A. Burns, (2009a), Three tenuous rings/arcs for three tiny moons, Icarus, 199, 378–386.

Hedman, M. M., P. D. Nicholson, M. R. Showalter, R. H. Brown, B. J. Buratti, R. N. Clark, (2009b), Spectral observations of the Enceladus plume with Cassini-VIMS, The Astrophysical Journal, 693, 1749–1762.

Hedman, M. M., J. A. Burns, M. S. Tiscareno, C. C. Porco, G. H. Jones, E. Roussos, N. Krupp, C. Paranicas, S. Kempf, (2007), The source of Saturn's G ring, Science, 317, 653–656.

Hillier, J. K., S. F. Green, N. McBride, N. Altobelli, F. Postberg, S. Kempf, J. Schwanethal, R. Srama, J. A. M. McDonnell, E. Grün, (2007a), Interplanetary dust detected by the Cassini CDA Chemical Analyzer, Icarus, 190, 643–654.

Hillier, J. K., S. F. Green, N. McBride, J. P. Schwanethal, F. Postberg, R. Srama, S. Kempf, G. Moragas-Klostermeyer, J. A. M. McDonnell, E. Grün, (2007b), The composition of Saturn's E ring, Monthly Notices of the Royal Astronomical Society, 377, 1588–1596.

Horányi, M., A. Juhasz, G. E. Morfill, (2008), Large-scale structure of Saturn's E-ring, Geophysical Research Letters, 35, L04203.

Horányi, M., (2000), Dust streams from Jupiter and Saturn, Physics of Plasmas, 7(10), 3847–3850.

Horányi, M., G. Morfill, E. Grün, (1993), Mechanism for the acceleration and ejection of dust grains from Jupiter's magnetosphere, Nature, 363, 144–146.

Horányi, M., J. Burns, D. Hamilton, (1992), The dynamics of Saturn's E ring particles, Icarus, 97, 248–259.

Hsu, H. W., J. Schmidt, S. Kempf, F. Postberg, G. Moragas-Klostermeyer, M. Seiß, H. Hoffmann, M. Burton, S.-Y. Ye, W. S. Kurth, M. Horányi, N. Khawaja, F. Spahn, D. Schirdewahn, J. O'Donoghue, L. Moore, J. Cuzzi, G. H. Jones, R. Srama, (2018), In situ collection of dust grains falling from Saturn's rings into its atmosphere, Science, 362(6410), eaat3185, doi: 10.1126/science.aat3185.

Hsu, H., M. Horányi, S. Kempf, (2017), On the time-dependent grain charging and its effects on ring-atmosphere interactions at Saturn, American Institute of Physics Conference Proceedings.

Hsu, H.-W., S. Kempf, S. V. Badman, W. S. Kurth, F. Postberg, R. Srama, (2016), Interplanetary magnetic field structure at Saturn inferred from nanodust measurements during the 2013 aurora campaign, Icarus, 263, 10–16.

Hsu, H.-W., F. Postberg, Y. Sekine, T. Shibuya, S. Kempf, M. Horányi, A. Juhasz, N. Altobelli, K. Suzuki, Y. Masaki, T. Kuwatani, S. Tachibana, S.-I. Sirono, G. Moragas-Klostermeyer, R. Srama, (2015), Ongoing hydrothermal activities within Enceladus, Nature, 519, 207–210.

Hsu, H.-W., K. C. Hansen, M. Horányi, S. Kempf, A. Mocker, G. Moragas-Klostermeyer, F. Postberg, R. Srama, B. Zieger, (2013a), Probing IMF using nanodust measurements from inside Saturn's magnetosphere, Geophysical Research Letters, 40, 2902–2906.

Hsu, H.-W., M. Horányi, S. Kempf, (2013b), Dust and spacecraft charging in Saturn's E ring, Earth, Planets, and Space, 65, 149–156.

Hsu, H.-W., M. Horányi, S. Kempf, E. Grün, (2012a), Spacecraft charging near Enceladus, Geophysical Research Letters, 39, 6108.

Hsu, H.-W., H. Krüger, F. Postberg, (2012b), Dynamics, composition, and origin of Jovian and Saturnian dust-stream particles, in Astrophysics and Space Science Library, (eds.) I. Mann, N. Meyer-Vernet, A. Czechowski, Volume 385, p. 77.

Hsu, H.-W., S. Kempf, F. Postberg, M. Trieloff, M. Burton, M. Roy, G. Moragas-Klostermeyer, R. Srama, (2011a), Cassini dust stream particle measurements during the first three orbits at Saturn, Journal of Geophysical Research, 116, A08213.

Hsu, H.-W., F. Postberg, S. Kempf, M. Trieloff, M. Burton, M. Roy, G. Moragas-Klostermeyer, R. Srama, (2011b), Stream particles as the probe of the dust-plasma-magnetosphere interaction at Saturn, Journal of Geophysical Research, 116, A09215.

Hsu, H., S. Kempf, C. M. Jackman, (2010a), Observation of Saturnian stream particles in the interplanetary space, Icarus, 206, 653–661.

Hsu, H., S. Kempf, F. Postberg, R. Srama, C. M. Jackman, G. Moragas-Klostermeyer, S. Helfert, E. Grün, (2010b), Interaction of the solar wind and stream particles, results from the Cassini dust detector, Twelfth International Solar Wind Conference, American Institute of Physics Conference Proceedings, 1216, 510–513.

Ingersoll, A. P. and S. P. Ewald, (2011), Total particulate mass in Enceladus plumes and mass of Saturn’s E ring inferred from Cassini ISS images, Icarus, 216, 492–506.

Jones, G. H., E. Roussos, N. Krupp, U. Beckmann, A. J. Coates, F. Crary, I. Dandouras et al. (2008), The dust halo of Saturn's largest icy moon, Rhea, Science 319, 5868, 1380–1384.

Juhasz, A. and M. Horányi, (2002), Saturn’s E ring, A dynamical approach, Journal of Geophysical Research, 107, 1–10.

Jurac, S., R. E. Johnson, J. D. Richardson, (2001), Saturn’s E ring and production of the Neutral Torus, Icarus, 149, 384–396.

Kempf, S., R. Srama, G. Moragas-Klostermeyer, J. Schmidt, F. Spahn, M. Horányi, (2012), Saturn’s egg-shaped E ring, in EGU General Assembly Conference Abstracts, (eds.) A. Abbasi and N. Giesen, 14, 11409.

Kempf, S., U. Beckmann, J. Schmidt, (2010), How the Enceladus dust plume feeds Saturn’s E ring, Icarus, 206, 446–457.

Kempf, S., (2008a), Interpretation of high rate dust measurements with the Cassini dust detector CDA, Planetary and Space Science, 56, 378–385.

Kempf, S., U. Beckmann, G. Moragas-Klostermeyer, F. Postberg, R. Srama, T. Economou, J. Schmidt, F. Spahn, E. Grün, (2008b), The E ring in the vicinity of Enceladus I, Spatial distribution and properties of the ring particles, Icarus, 193, 420–437.

Kempf, S., U. Beckmann, R. Srama, M. Horányi, S. Auer, E. Grün, (2006), The electrostatic potential of E ring particles, Planetary and Space Science, 54, 999–1006.

Kempf, S., R. Srama, M. Horányi, M. Burton, S. Helfert, G. Moragas-Klostermeyer, M. Roy, E. Grün, (2005a), High-velocity streams of dust originating from Saturn, Nature, 433, 289–291.

Kempf, S., R. Srama, F. Postberg, M. Burton, S. F. Green, S. Helfert, J. K. Hillier, N. McBride, J. A. M. McDonnell, G. Moragas-Klostermeyer, M. Roy, E. Grün, (2005b), Composition of Saturnian stream particles, Science, 307, 1274–1276.

- - - - - - - - - - - - - -

Kempf, S., R. Srama, N. Altobelli, S. Auer, V. Tschernjawski, J. Bradley, M. Burton, S. Helfert, T. Johnson, H. Krüger, G. Moragas-Klostermeyer, E. Grün, (2004), Cassini between Earth and asteroid belt, First in-situ charge measurements of interplanetary grains, Icarus, 171, 317–335.

Khawaja, N., F. Postberg, J. Schmidt, (2017), The compositional profile of the Enceladus ice plume from the latest Cassini flybys, Lunar and Planetary Science Conference, 2005.

Krivov, A. V., M. Sremcevic, F. Spahn, V. V. Dikarev, K. V. Kholshevnikov, (2003), Impact-generated dust clouds around planetary satellites, Spherically symmetric case, Planetary and Space Science, 51, 251–269.

Krüger, H., P. Geissler, M. Horányi, A. Graps, S. Kempf, R. Srama, G. Moragas-Klostermeyer, R. Moissl, T. Johnson, E. Grün, (2003a), Jovian dust streams, A monitor of Io's volcanic plume activity, Geophysical Research Letters, 30(21), 2101.

Krüger, H., M. Horányi, E. Grün, (2003b), Jovian dust streams, Probes of the Io plasma torus, Geophysical Research Letters, 30(2), 1058.

Krüger, H., A. Krivov, D. Hamilton, E. Grün, (1999), Detection of an impact-generated dust cloud around Ganymede, Nature, 399, 558–560.

Krupp, N., E. Roussos, C. Paranicas, D. G. Mitchell, P. Kollmann, S. Ye, W. S. Kurth, K. K. Khurana, R. Perryman, H. Waite, R. Srama, D. C. Hamilton, (2018), Energetic electron measurements near Enceladus by Cassini during 2005–2015, Icarus, 306, 256–274.

Landgraf, M., H. Krüger, N. Altobelli, E. Grün, (2003), Penetration of the heliosphere by the interstellar dust stream during solar maximum, Journal of Geophysical Research, 108, 5–1.

McBride, N., J. K. Hillier, S. F. Green, R. Srama, S. Kempf, F. Postberg, G. Moragas-Klostermeyer, J. A. M. McDonnell, E. Grün, (2007), Cassini Cosmic Dust Analyzer, Composition of dust at Saturn, Dust in Planetary Systems, 643, 107–110.

Moore, L., J. O'Donoghue, I. Müller-Wodarg, M. Galand, M. Mendillo, (2015), Saturn ring rain, Model estimates of water influx into Saturn's atmosphere, Icarus, 245, 355–366.

Morooka, M. W., J.-E. Wahlund, A. I. Eriksson, W. M. Farrell, D. A. Gurnett, W. S. Kurth, A. M. Persoon, M. Shafiq, M. André, M. K. G. Holmberg, (2011), Dusty plasma in the vicinity of Enceladus, Journal of Geophysical Research (Space Physics), 116, 12221.

Nicholson, P. D., M. R. Showalter, L. Dones, (1996), Observations of Saturn's ring-plane crossing in August and November, Science, 272, 509–516.

O'Donoghue, J., T. S. Stallard, H. Melin, G. H. Jones, S. W. H. Cowley, S. Miller, K. H. Baines, J. S. D. Blake, (2013), The domination of Saturn's low-latitude ionosphere by ring 'rain', Nature, 496, 193–195.

Poppe, A. R. and M. Horányi, (2012), On the Edgeworth-Kuiper Belt dust flux to Saturn, Geophysical Research Letters, 39, L15104.

Postberg, F., N. Khawaja, B. Abel, G. Choblet, C. Glein, M. Gudipati, B. L. Henderson, H. Hsu, S. Kempf, F. Klenner, G. Moragas-Klostermeyer, B. Magee, L. Nölle, M. Perry, R. Reviol,

J. Schmidt, R. Srama, F. Stolz, G. Tobie, M. Trieloff, J. H. Waite, (2018), Macromolecular organic compounds from the depths of Enceladus, Nature, 558(7711), 564.

Postberg, F., J. Schmidt, J. Hillier, S. Kempf, R. Srama, (2011), A salt-water reservoir as the source of a compositionally stratified plume on Enceladus, Nature, 474, 620–622.

Postberg, F., S. Kempf, D. Rost, T. Stephan, R. Srama, M. Trieloff, A. Mocker, M. Goerlich, (2009a), Discriminating contamination from particle components in spectra of Cassini's dust detector CDA, Planetary and Space Science, 57, 1359–1374.

Postberg, F., S. Kempf, J. Schmidt, N. Brilliantov, A. Beinsen, B. Abel, U. Buck, R. Srama, (2009b), Sodium salts in E-ring ice grains from an ocean below the surface of Enceladus, Nature, 459, 1098–1101.

Postberg, F., S. Kempf, J. K. Hillier, R. Srama, S. F. Green, N. McBride, E. Grün, (2008), The E-ring in the vicinity of Enceladus II, Signatures of Enceladus in the elemental composition of E-ring particles, Icarus, 193, 438–454.

Postberg, F., S. Kempf, R. Srama, S. F. Green, J. K. Hillier, N. McBride, E. Grün, (2006), Composition of Jovian dust stream particles, Icarus, 183, 122–134.

Schenk, P., D. P. Hamilton, R. E. Johnson, W. B. McKinnon, C. Paranicas, J. Schmidt, M. R. Showalter, (2011), Plasma, plumes and rings, Saturn system dynamics as recorded in global color patterns on its midsize icy satellites, Icarus, 211, 740–757.

Schmidt, J., N. Brilliantov, F. Spahn, S. Kempf, (2008), Slow dust in Enceladus' plume from condensation and wall collisions in tiger stripe fractures, Nature, 451, 685–688.

Seiß, M., R. Srama, K.-L. Sun, M. Seiler, G. Moragas-Klostermeyer, S. Kempf, F. Spahn, (2014), Pallene dust torus observations by the Cosmic Dust Analyzer, European Planetary Science Congress, 9, EPSC2014–375.

Sekine, Y., T. Shibuya, F. Postberg, H. Hsu, K. Suzuki, Y. Masaki, T. Kuwatani, M. Mori, P. K. Hong, M. Yoshizaki, S. Tachibana, S.-I Sirono, (2015), High-temperature water–rock interactions and hydrothermal environments in the chondrite-like high-temperature water-rock interactions and hydrothermal environments in the chondrite-like core of Enceladus, Nature Communications, 6(8604).

Showalter, M. R., J. N. Cuzzi, S. M. Larson, (1991), Structure and particle properties of Saturn's E ring, Icarus, 94, 451–473.

Southworth, B. S., S. Kempf, J. Spitale, (2019), Surface deposition of the Enceladus plume and the zenith angle of emissions, Icarus, 319, 33–42.

Spahn, F., N. Albers, M. Hörning, S. Kempf, A. V. Krivov, M. Makuch, J. Schmidt, M. Seiß, M. Sremcevic, (2006a), E ring dust sources, Implications from Cassini's dust measurements, Planetary and Space Science, 54, 1024–1032.

Spahn, F., J. Schmidt, N. Albers, M. Hörning, M. Makuch, M. Seiß, S. Kempf, R. Srama, V. Dikarev, S. Helfert, G. Moragas-Klostermeyer, A. V. Krivov, M. Sremcevic, A. J. Tuzzolino,

T. Economou, E. Grün, (2006b), Cassini dust measurements at Enceladus and implications for the origin of the E ring, Science, 311, 1416–1418.

Spencer, J. R., S. A. Stern, A. F. Cheng, H. A. Weaver, D. C. Reuter, K. Retherford, A. Lunsford, J. M. Moore, O. Abramov, R. M. C. Lopes, J. E. Perry, L. Kamp, M. Showalter, K. L. Jessup, F. Marchis, P. M. Schenk, C. Dumas, (2007), Io volcanism seen by New Horizons, A major eruption of the Tvashtar volcano, Science, 318, 240–.

Srama, R., S. Kempf, G. Moragas-Klostermeyer, N. Altobelli, S. Auer, U. Beckmann, S. Bugiel, M. Burton, T. Economomou, H. Fechtig, K. Fiege, S. F. Green, M. Grande, O. Havnes, J. K. Hillier, S. Helfert, M. Horányi, S. Hsu, E. Igenbergs, E. K. Jessberger, T. V. Johnson, E. Khalisi, H. Krüger, G. Matt, A. Mocker, P. Lamy, G. Linkert, F. Lura, D. Möhlmann, G. E. Morfill, K. Otto, F. Postberg, M. Roy, J. Schmidt, G. H. Schwehm, F. Spahn, V. Sterken, J. Svestka, V. Tschernjawski, E. Grün, H.-P. Röser, (2011), The Cosmic Dust Analyzer onboard Cassini, Ten years of discoveries, CEAS Space Journal, 2, 3–16.

Srama, R., S. Kempf, G. Moragas-Klostermeyer, S. Helfert, T. J. Ahrens, N. Altobelli, S. Auer, U. Beckmann, J. G. Bradley, M. Burton, V. V. Dikarev, T. Economou, H. Fechtig, S. F. Green, M. Grande, O. Havnes, J. K. Hillier, M. Horányi, E. Igenbergs, E. K. Jessberger, T. V. Johnson, H. Krüger, G. Matt, N. McBride, A. Mocker, P. Lamy, D. Linkert, G. Linkert, F. Lura, J. A. M. McDonnell, D. Mohlmann, G. E. Morfill, F. Postberg, M. Roy, G. H. Schwehm, F. Spahn, J. Svestka, V. Tschernjawski, A. J. Tuzzolino, R. Wäsch, E. Grün, (2006), In situ dust measurements in the inner Saturnian system, Planetary and Space Science, 54, 967–987.

Srama, R., M. Stübig, E. Grün, (2004), Laboratory detection of organic dust with the Cassini-CDA instrument, Advances in Space Research, 33, 1289–1293.

Sremcevic, M., A. V. Krivov, F. Spahn, (2003), Impact-generated dust clouds around planetary satellites, asymmetry effects, Planetary and Space Science, 51, 455–471.

Staubach, P., E. Grün, R. Jehn, (1997), The meteoroid environment near earth, Advances in Space Research, 19, 301–308.

Sterken, V. J., N. Altobelli, S. Kempf, G. Schwehm, R. Srama, E. Grün, (2012), The flow of interstellar dust into the solar system, Astronomy and Astrophysics, 538, A102.

Sun, K.-L., M. Seiß, M. M. Hedman, F. Spahn, (2017), Dust in the arcs of Methone and Anthe, Icarus, 284, 206–215.

Verbiscer, A., R. French, M. Showalter, P. Helfenstein, (2007), Enceladus, Cosmic graffiti artist caught in the act, Science, 315, 815.

Ye, S.-Y., D. A. Gurnett, W. S. Kurth, (2016), In-situ measurements of Saturn's dusty rings based on dust impact signals detected by Cassini RPWS, Icarus, 279, 51–61.

Ye, S.-Y., D. A. Gurnett, W. S. Kurth, T. F. Averkamp, S. Kempf, H.-W. Hsu, R. Srama, E. Grün, (2014), Properties of dust particles near Saturn inferred from voltage pulses induced by dust impacts on Cassini spacecraft, Journal of Geophysical Research, 119, 6294–6312.